NONSYMMETRIC TRANSVERSE VIBRATIONS OF TRUNCATED CONICAL SHELLS

U. S. Lindholm
W. C. L. Hu

Technical Report No. 3
Contract NASr-94(06)
SwRI Project No. 02-1504

Prepared for

National Aeronautics and Space Adminstration
Washington 25, D. C.

March 31, 1965

SOUTHWEST RESEARCH INSTITUTE
SAN ANTONIO HOUSTON

NONSYMMETRIC TRANSVERSE VIBRATIONS OF TRUNCATED CONICAL SHELLS

U. S. Lindholm
W. C. L. Hu

Technical Report No. 3
Contract NASr-94(06)
SwRI Project No. 02-1504

Prepared for

National Aeronautics and Space Administration
Washington 25, D. C.

March 31, 1965

APPROVED:

H. Norman Abramson, Director
Department of Mechanical Sciences

SUMMARY

A combined theoretical and experimental study is presented of resonant frequencies and associated mode shapes of truncated conical shells over a wide range of geometrical and modal parameters. The theoretical analysis incorporates the effects of bending and membrane rigidity, and of inertia terms due to transverse motion as well as meridional and circumferential in-plane motion. The experimental results were obtained for four conical shell models, with semi-vertex angle 14°, 30°, 45°, and 60°. The correlation of both resonant frequencies and mode shapes is very good.

Author

TABLE OF CONTENTS

LIST OF ILLUSTRATIONS

SYMBOLS

A^{ij}, B^{ij}	operators, element at i^{th} row and j^{th} column of operator matrix A, B, respectively
A^{ij}_{km}, B^{ij}_{km}	element at k^{th} row and m^{th} column of the submatrix $[A^{ij}_{km}]$, $[B^{ij}_{km}]$, respectively
a, b	radius of the major and minor base, respectively
a_m, b_m, c_m, d_m	Fourier coefficients of mode functions
C	$= Eh/(1-\nu^2)$, extensional modulus
D	$= Eh^3/12(1-\nu^2)$, flexural modulus
$\mathscr{D}$	$= d/dx$, differential operator
E	Young's modulus
H^{*ij}	operator, element at i^{th} row and j^{th} column of operator matrix H^*
h	thickness of shell
k_s	$= \kappa(1-\nu)/2$, shear constant
L	$= \log(s_2/s_1) = \log(a/b)$, logarithmic completeness parameter
M_s, M_θ, $M_{s\theta}$	stress couple resultants
N_s, N_θ, $N_{s\theta}$	stress resultants
n	circumferential wave number
Q_s, Q_θ	transverse shearing stress resultants
s	distance along meridian, measured from apex
t	time
u, v, w	displacements of middle surface
x	$= \log(s_2/s)$, meridional coordinate

SYMBOLS (Cont'd)

α	semivertix angle of cone
β_s, β_θ	angular displacements of normal to middle surface
ϵ	$= h^2/12a^2$, dimensionless thickness parameter
θ	circumferential coordinate angle
κ	shear constant
μ	$= m\pi/L$
ν	Poisson's ratio
ρ	mass density
Ω	$= \omega a\sqrt{\rho(1-\nu^2)/E}$, dimensionless frequency parameter
ω	natural frequency in rad/sec

INTRODUCTION

The determination of resonant frequencies and the associated mode shapes for thin-walled, shell structures has become an increasingly important problem in the design and analysis of complex space structures. However, the great number and variety of modes in which these shells can vibrate makes the problem rather complicated and involved. Only for shells of relatively simple geometry, such as the circular cylinder or sphere, can the mode shapes be given explicitly in terms of elementary or tabulated functions. In general, the curvature of the shell varies from point to point, and the governing differential equations contain variable coefficients, are non-separable and do not have explicit solutions.

In the present paper the truncated conical shell is treated. The circular cone has probably the simplest geometry of all the rotationally symmetric shells with nonconstant curvature and has obvious importance in space structures and other applications. The literature on conical shells has been reviewed in [1]* and [2] and will not be repeated here. It has been pointed out in [2] that the analytical techniques employed for solving free vibrations of conical shells have been limited to either energy methods [3 - 9], or numerical integration procedures [10 - 13]. In many cases, the assumptions used have restricted the solution to nearly cylindrical shells

*Numbers in brackets refer to references cited at the end of this report.

[5, 6, and 9]. Although both polynomial and trigonometric expansions can be used for the mode shapes in Rayleigh-Ritz methods, the resulting frequency will not acquire satisfactory accuracy unless a sufficient number of terms are retained in these expansions. A distressing aspect of the shell vibration problem is the fact that a large number of widely different modes may respond to a given excitation. Therefore, it would appear essential to identify all of the resonances within the frequency spectrum of interest in order to avoid, if possible, large deflections or stresses. Above the minimum resonant frequency, the density of resonance for thin shells is generally very high, so that rather accurate analysis is needed if they are to be avoided.

In [2], Hu has presented a method of solution for the truncated cone with homogeneous boundary conditions which has the great advantage that it retains the mathematical features of the vibration problem in that the natural frequencies and mode functions are obtained as the eigenvalues and associated eigenvectors of a coefficient matrix. Reference [2] presents the general formulation of the problem with numerical results presented for membrane solutions of axisymmetric modes only. In this paper, solutions are obtained for nonsymmetric transverse modes, including both the membrane and bending stiffness. These modes, referred to by some authors as "bell modes" or "breathing modes," generally have more physical significance and practical importance than the many other modes possible. In general,

these modes possess the following characteristic features: (1) the transverse motion predominates; thus, the vibration is usually visible and audible, (2) the resonant frequencies form the lowest group in the entire frequency spectrum, and (3) the response of normal displacement to external disturbance is usually larger than the response in other modes; therefore, from the structural view-point, resonance of transverse modes should be carefully avoided.

In order to verify the degree of validity of the theoretical predictions, experiments were performed on four different shell models having widely different cone angle. Correlation is presented for both resonant frequencies and mode shapes for the shells freely-supported at both edges.

ANALYSIS

Matrix Form of Governing Differential Equations

A set of differential equations in terms of displacements governing the free vibrations of truncated conical shells has been derived in [2]*. These equations incorporate the effects of both bending and membrane stresses, and retain inertia terms for both the transverse motion and the in-plane, meridional and circumferential motion. The terms corresponding to rotary inertia and transverse shear deformation are included for the meridional direction only, analogous terms for the circumferential direction being neglected. A matrix equation for the displacement vector $U^* = \{u_n \; v_n \; w_n \; \beta_{sn}\}$ is obtained in the form

$$H^* U^* = \Omega^2 U^* \tag{1}$$

where H^* is a (4×4) operator matrix containing the differential operator, and Ω is the dimensionless frequency parameter

$$\Omega = \omega a \sqrt{\rho(1 - \nu^2)/E} \tag{2}$$

The operators H^{*ij}, i, j, = 1, 2, 3, 4, of the matrix H^* are given in Appendix I. The dimensionless mode functions u_n, v_n, w_n and β_{sn} are defined by the following separation process:

*See particularly pages 3-12, 17-22.

$$\begin{Bmatrix} u \\ w \\ \beta_s \end{Bmatrix} = \begin{Bmatrix} au_n \\ aw_n \\ \beta_{sn} \end{Bmatrix} \sin(n\theta + \theta_o) \cos \omega t \tag{3}$$

$$v = av_n \cos(n\theta + \theta_o) \cos \omega t \tag{4}$$

The shell geometry and coordinate system is defined in Figure 1.

The four equations in (1) are coupled second-order differential equations with variable coefficients. The independent variable can be either the meridional distance s measured from the apex, or the transformed variable,

$$x = \log\left(\frac{s_2}{s}\right) \tag{5}$$

which is dimensionless and will be used throughout this analysis. It is evident that the mode functions are continuous, smooth functions of x in the interval $0 \leqslant x \leqslant L$ where

$$L = \log\left(\frac{s_2}{s_1}\right) \tag{6}$$

It might be remarked that if the semi-vertex angle $\alpha = 0$ (cylindrical shells), the mode functions are known to be expressible in trigonometric and exponential functions of s; while if $\alpha = \pi/2$ (annular plates), the transverse vibration is uncoupled and the mode function w_n is expressible in Bessel functions of s. In the general case, however, the mode functions cannot be expressed in terms of any known tabulated functions and must be solved by some numerical process. In the present analysis they are expanded into Fourier series with the coefficeints determined by a Galerkin procedure.

Calculation of Frequencies and Modes

The boundary conditions for shell problems are always hard to prescribe, especially to represent experimental or actual conditions. Two different end conditions will be discussed here, both being simply supported with reference to the transverse displacement but differing with regard to the in-plane meridional restraint. In the first case the displacement in the meridional direction, u, is taken as zero at the boundaries, and then is relaxed in the second case. In both cases, the circumferential and transverse displacements as well as the moment in the meridional direction are assumed zero. The first condition will be referred to as simply-supported and the second freely-supported.

Simply-supported edges with meridional constraint. The boundary conditions are, $u_n = v_n = w_n = M_{sn} = 0$, at $x = 0, L$. The last condition, $M_{sn} = 0$, is equivalent to

$$\frac{d\beta_{sn}}{dx} - \nu\beta_{sn} = 0, \text{ at } x = 0, L. \tag{7}$$

Therefore, the following truncated Fourier expansions will satisfy all the boundary conditions term by term

$$u_n = \sum_{m=1}^{M1} a_m \sin\frac{m\pi x}{L} \tag{8a}$$

$$v_n = \sum_{m=1}^{M2} b_m \sin\frac{m\pi x}{L} \tag{8b}$$

$$w_n = \sum_{m=1}^{M_3} c_m \sin \frac{m\pi x}{L} \tag{8c}$$

$$\beta_{sn} = e^{\nu x}\left[\frac{d_o}{2} + \sum_{m=1}^{M_4} d_m \cos \frac{m\pi x}{L}\right] \tag{8d}$$

where $M_1, \ldots, M_4$ are properly chosen integers. For simplicity, we will use a new variable

$$\beta^*_{sn} = e^{-\nu x}\beta_{sn} = \frac{d_o}{2} + \sum_{m=1}^{M_4} d_m \cos \frac{m\pi x}{L} \tag{8d'}$$

Then (1) can be transformed to

$$[A^{ij}] \begin{Bmatrix} u_n \\ v_n \\ w_n \\ \beta^*_{sn} \end{Bmatrix} = \Omega^2 \begin{Bmatrix} u_n \\ v_n \\ w_n \\ \beta^*_{sn} \end{Bmatrix}, i, j = 1, \ldots, 4 \tag{9}$$

where

$$[A^{ij}] = \begin{bmatrix} H^{*11} & H^{*12} & H^{*13} & H^{*14}e^{\nu x} \\ H^{*21} & H^{*22} & H^{*23} & H^{*24}e^{\nu x} \\ H^{*31} & H^{*32} & H^{*33} & H^{*34}e^{\nu x} \\ e^{-\nu x}H^{*41} & e^{-\nu x}H^{*42} & e^{-\nu x}H^{*43} & e^{-\nu x}H^{*44}e^{\nu x} \end{bmatrix} \tag{10}$$

Note that the operators H^{*ij} and $e^{\nu x}$ are in general not commutative.*

We assume that the Fourier expansions (8) are termwise differentiable twice. Substitution of (8) into (9) and application of the Galerkin procedure yields the following matrix equation governing the Fourier coefficients a's, b's, c's, and d's:

*Refer to [2], pp. 12-17

$$
\begin{array}{c}
\\
M_1 \\
M_2 \\
M_3 \\
M_4+1
\end{array}
\left\{
\begin{bmatrix}
\overbrace{\begin{bmatrix} A_{km}^{11} \end{bmatrix}}^{M_1} & \overbrace{\begin{bmatrix} A_{km}^{12} \end{bmatrix}}^{M_2} & \overbrace{\begin{bmatrix} A_{km}^{13} \end{bmatrix}}^{M_3} & \overbrace{\begin{bmatrix} A_{km}^{14} \end{bmatrix}}^{M_4+1} \\
\begin{bmatrix} A_{km}^{21} \end{bmatrix} & \begin{bmatrix} A_{km}^{22} \end{bmatrix} & \begin{bmatrix} A_{km}^{23} \end{bmatrix} & \begin{bmatrix} A_{km}^{24} \end{bmatrix} \\
\begin{bmatrix} A_{km}^{31} \end{bmatrix} & \begin{bmatrix} A_{km}^{32} \end{bmatrix} & \begin{bmatrix} A_{km}^{33} \end{bmatrix} & \begin{bmatrix} A_{km}^{34} \end{bmatrix} \\
\begin{bmatrix} A_{km}^{41} \end{bmatrix} & \begin{bmatrix} A_{km}^{42} \end{bmatrix} & \begin{bmatrix} A_{km}^{43} \end{bmatrix} & \begin{bmatrix} A_{km}^{44} \end{bmatrix}
\end{bmatrix}
\begin{Bmatrix} a_1 \\ \vdots \\ b_1 \\ \vdots \\ c_1 \\ \vdots \\ d_o \\ \vdots \end{Bmatrix}
= \Omega^2
\begin{Bmatrix} a_1 \\ \vdots \\ b_1 \\ \vdots \\ c_1 \\ \vdots \\ d_o \\ \vdots \end{Bmatrix}
\qquad (11)
$$

where

$$
A_{km}^{ij} = \frac{2}{L}\int_0^L \sin\frac{k\pi x}{L}\left(A^{ij}\sin\frac{m\pi x}{L}\right)dx \qquad i,j = 1,\ 2,\ 3
$$

$$
A_{km}^{i4} = \frac{2}{L}\int_0^L \sin\frac{k\pi x}{L}\left(A^{i4}\cos\frac{m\pi x}{L}\right)dx \qquad i = 1,\ 2,\ 3
$$

$$
A_{km}^{4j} = \frac{2}{L}\int_0^L \cos\frac{k\pi x}{L}\left(A^{4j}\sin\frac{m\pi x}{L}\right)dx \qquad j = 1,\ 2,\ 3
$$

$$
A_{km}^{44} = \frac{2}{L}\int_0^L \cos\frac{k\pi x}{L}\left(A^{44}\cos\frac{m\pi x}{L}\right)dx
$$

Note that whenever m = 0, $\cos\frac{m\pi x}{L}$ should be replaced by 1/2. The sixteen algebraic formulas which generate the submatrices $\left[A_{km}^{ij}\right]$, i, j = 1, . . . , 4, are given in Appendix II. The eigenvalues and eigenvectors of the coefficient matrix, which can be readily calculated on a digital computer, give the natural frequencies and associated mode functions of the simply-supported conical shell.

Freely supported edges without meridional constraint. From numerical results computed by applying the matrix equation (11), it was found that the above formulation yielded higher frequencies than those measured in the experiments. A closer examination of the edge supports used in the experiments indicated that little constraint was provided to the meridional, in-plane motion. Therefore, the meridional constraint, $u_n = 0$, at $x = 0, L$, was released to obtain a better description of the experimental boundary condition and, at the same time, illustrate the relative influence of the longitudinal constraint.

Replacing $u_n = 0$ by $N_{sn} = 0$, or equivalently

$$\frac{du_n}{dx} - \nu u_n = 0, \text{ at } x = 0, L \tag{12}$$

the series (8a) should be replaced by

$$u_n = e^{\nu x}\left[\frac{a_o}{2} + \sum_{m=1}^{M_1} a_m \cos\frac{m\pi x}{L}\right]$$

In addition to using (8d'), define a new variable

$$u_n^* = e^{-\nu x}\left[\frac{a_o}{2} + \sum_{m=1}^{M_1} a_m \cos\frac{m\pi x}{L}\right] \tag{8a'}$$

Then (1) can be transformed to

$$[B^{ij}]\begin{Bmatrix} u_n^* \\ v_n \\ w_n \\ \beta_{sn}^* \end{Bmatrix} = \Omega^2 \begin{Bmatrix} u_n^* \\ v_n \\ w_n \\ \beta_{sn}^* \end{Bmatrix} \tag{13}$$

where

$$[B^{ij}] = \begin{bmatrix} e^{-\nu x}H^{*11}e^{\nu x} & e^{-\nu x}H^{*12} & e^{-\nu x}H^{*13} & e^{-\nu x}H^{*14}e^{\nu x} \\ H^{*21}e^{\nu x} & H^{*22} & H^{*23} & H^{*24}e^{\nu x} \\ H^{*31}e^{\nu x} & H^{*32} & H^{*33} & H^{*34}e^{\nu x} \\ e^{-\nu x}H^{*41}e^{\nu x} & e^{-\nu x}H^{*42} & e^{-\nu x}H^{*43} & e^{-\nu x}H^{*44}e^{\nu x} \end{bmatrix} \tag{14}$$

Substituting (8a', b, c, and d') into (13) and applying the Galerkin procedure, we can readily obtain a matrix equation similar to (11)

$$\begin{bmatrix} [B^{11}_{km}] & [B^{12}_{km}] & [B^{13}_{km}] & [B^{14}_{km}] \\ [B^{21}_{km}] & [B^{22}_{km}] & [B^{23}_{km}] & [B^{24}_{km}] \\ [B^{31}_{km}] & [B^{32}_{km}] & [B^{33}_{km}] & [B^{34}_{km}] \\ [B^{41}_{km}] & [B^{42}_{km}] & [B^{43}_{km}] & [B^{44}_{km}] \end{bmatrix} \begin{Bmatrix} a_o \\ \vdots \\ b_1 \\ \vdots \\ c_1 \\ \vdots \\ d_o \\ \vdots \end{Bmatrix} = \Omega^2 \begin{Bmatrix} a_o \\ \vdots \\ b_1 \\ \vdots \\ c_1 \\ \vdots \\ d_o \\ \vdots \end{Bmatrix} \tag{15}$$

where

$$B^{ij}_{km} = \frac{2}{L}\int_0^L \cos\frac{k\pi x}{L}\left[B^{ij}\cos\frac{m\pi x}{L}\right]dx \qquad i,j = 1, 4$$

$$= \frac{2}{L}\int_0^L \cos\frac{k\pi x}{L}\left[B^{ij}\sin\frac{m\pi x}{L}\right]dx \qquad i = 1, 4, \quad j = 2, 3$$

$$= \frac{2}{L}\int_0^L \sin\frac{k\pi x}{L}\left[B^{ij}\cos\frac{m\pi x}{L}\right]dx \qquad i = 2, 3 \quad j = 1, 4$$

$$= \frac{2}{L}\int_0^L \sin\frac{k\pi x}{L}\left[B^{ij}\sin\frac{m\pi x}{L}\right]dx \qquad i, j = 2, 3$$

As mentioned before, whenever $m = 0$, $\cos\frac{m\pi x}{L}$ should be replaced by $1/2$. The sixteen algebraic formulas which generate the submatrices $\left[B^{ij}_{km}\right]$, $i, j = 1, \ldots, 4$, are given in Appendix III.

Numerical Procedure

It can be seen from the coefficient matrices $\left[A^{ij}_{km}\right]$ or $\left[B^{ij}_{km}\right]$ that the frequency parameter Ω and the mode functions depend on six parameters:

$$\Omega = \Omega\left(\alpha, \frac{s_2}{s_1}, \frac{h}{a}, \nu, n, m\right) \tag{16}$$

Poisson's ratio ν is taken as 0.3 in all calculations. The first three are geometric parameters and have prescribed values for the four models tested. These are given in Table 1.

TABLE 1.

Model No.	α	s_2/s_1	h/a	a (in.)
1	14.2°	2.23	0.00166	6.07
2	30.2°	2.27	0.00127	7.95
3	45.1°	2.25	0.00112	8.96
4	60.5°	2.25	0.00101	10.00

The circumferential wave number n was assigned selected integer values ranging from 3 to 28, to cover all modes being excited in the experiments. The number of terms $M_1, \ldots, M_4$, retained in the Fourier series is determined by the accuracy requirement. When n is not too large, a typical set is $M_1 = 4$, $M_2 = 4$, $M_3 = 5$, $M_4 = 6$, which yields a (21×21) coefficient matrix $\left[B^{ij}_{km}\right]$. This matrix is then inverted and the two largest eigenvalues are calculated by iteration, giving the two lowest natural

frequencies and associated modes, m = 1, 2. For very large values of n (say 24-28), it was found that a (28 $\times$ 28) matrix was needed to predict the frequencies with reasonable accuracy. No attempt was made to calculate the higher modes with greater accuracy because of the limited available computer storage capacity.

EXPERIMENTAL APPARATUS AND PROCEDURE

In order to verify the accuracy of the numerical procedures outlined in the preceding section, experiments were run on four shell models having the geometries described in Table 1. The experiments were similar to those described in [13] for cylindrical shells. The essential features of the experiments are that the steel shells are driven by a pulsed magnetic field, and the transverse displacement is measured by a noncontacting probe. In this manner, neither the excitation nor the measuring system adds additional mass or stiffness to the thin shell. Mapping of the transverse displacement mode shape allows direct correlation with the eigenvectors as well as the eigenvalues calculated from the appropriate coefficient matrices.

The shell models were formed from 0.010-inch thick rolled steel shim stock. The cones were formed from the flat sheet with one welded seam along a generator of the cone. This seam was arc-welded with a butt-joint so that a negligible discontinuity was formed in the shell.

A schematic of the experimental apparatus and instrumentation is shown in Figure 2, and a general view of the setup in Figure 3. The shell models are supported from a mandrel of a vertically mounted lathe bed. The boundary support shown in Figure 2 is that used to simulate the freely supported edge condition. The right-angle groove in the circular plate

supporting the lower end is machined to a close tolerance fit with the small radius b of the shell. The upper circular plate is positioned with a slight axial load to give a line support around the large radius a of the shell. The only in-plane restraint is the slight friction between the shell and the support.

Excitation to the shells was produced by a pulsed magnetic field from two small electromagnets located at opposite ends of a diameter of the shell. The frequency of the excitation was controlled by an oscillator driving the electromagnets through a power amplifier. In order to optimize the excitation of each mode, a phase control is added so that the two electromagnets can be operated either in-phase or out-of-phase depending upon the circumferential wave number n being either even or odd. The position of the excitation along a generator (s direction) of the shell is also adjustable so that various axial modes may be optimally excited.

The transverse displacement w is mapped with an inductance type displacement probe, mounted on a long lead screw so that it can traverse the shell in the s direction. The entire shell and excitation system may be rotated 360° on the central mandrel allowing a circumferential mode shape plot also. For direct plotting of the mode shapes, the position of the displacement probe with respect to the shell is given by a rotary potentiometer on the mandrel and a resistance slide wire on the lead screw assembly. The output signal from the displacement detector is conditioned through a tracking filter, tuned to the excitation frequency. The filtered output signal

can be recorded on either an oscilloscope, frequency counter, or x-y pen recorder for mode shape plots.

Resonance is determined as the frequency at which maximum transverse amplitude response is obtained. The accuracy of this method depends upon the sharpness of the amplitude-frequency response curves which, for low damping structures such as the shells tested, is sufficient to distinguish resonances separated by only a few cycles per second. Frequencies are read from an electronic frequency counter. Modes may be identified most easily by observing the phase relationship between the driving signal from the oscillator and the response signal from the displacement detector. Upon crossing a nodal line the phase shifts 180° and is easily detected by the rotation of the Lissajous figure on the x-y oscilloscope. Mode shapes can be plotted directly on an x-y pen recorder, with the rectified displacement amplitude on the y axis and the circumferential or meridional position on the x axis.

EXPERIMENTAL RESULTS AND CORRELATION

Resonant Frequencies

The resonant frequencies for the freely-supported cones are presented graphically in Figures 4, 5, 6, and 7 for the four shell models given in Table 1. The primary geometrical parameter being varied is the cone angle α; however, the thickness parameter h/a is also varied to some extent in order to maintain models of reasonable dimensions. The non-dimensional frequency parameter Ω is plotted against the circumferential wave number n. The theoretical natural frequencies are indicated by the solid, continuous curves, although it should be noted that n is a discrete parameter having only integer values. The theoretical and experimental frequencies are also given in Table 2.

The correlation between theory and experiment is seen to be quite good, particularly for the lowest axial mode, $m = 1$. The divergence between theory and experiment that does exist has two primary causes; namely, satisfaction of the assumed boundary conditions, and the finite truncation of the Fourier expansions for the mode functions. The mathematical and experimental boundary conditions have been described in preceding paragraphs. A problem arises in prescribing the in-plane displacements, u and v. For the 45° cone (Figure 6), two sets of theoretical curves are calculated and plotted, one being simply-supported and the

TABLE 2. THEORETICAL AND EXPERIMENTAL NATURAL FREQUENCIES, Ω, FOR CONICAL SHELLS TESTED

n \ m	1		2		3	4
	Theo	Exper	Theo	Exper	Exper	Exper
	Shell Model No. 1 (α = 14.2°)					
3	0.130	0.121	0.387			
4	0.0846	0.0756	0.258			
5		0.0582		0.180		
6	0.0575	0.0534	0.141	0.138		
7		0.0567		0.118		
8	0.0660	0.0640	0.110	0.108	0.177	
9		0.0735		0.114	0.166	
10	0.0849	0.0832	0.127	0.124	0.169	0.216
11		0.0934		0.135	0.179	
12	0.109	0.106	0.164	0.144	0.187	0.231
13		0.120		0.160	0.197	
14	0.141	0.132	0.209	0.174	0.213	0.254
15		0.146		0.189	0.226	
16	0.179	0.163	0.260	0.203	0.246	
17		0.181		0.223	0.262	
18	0.223	0.200	0.319	0.241		
19						
20	0.259	0.236	0.348			
	Shell Model No. 2 (α = 30.2°)					
4	0.236		0.578			
5		0.157				
6	0.130	0.122	0.360			
7		0.098				
8	0.095	0.090	0.244	0.232		
9		0.088		0.204		
10	0.096	0.092	0.193	0.187		
11		0.101		0.179		
12		0.109				
13		0.117		0.189	0.260	
14	0.133	0.130	0.206	0.200	0.268	
15		0.141		0.209	0.277	
16	0.155	0.153	0.230	0.224	0.290	0.355
17		0.167		0.237	0.299	0.362

TABLE 2. THEORETICAL AND EXPERIMENTAL NATURAL FREQUENCIES, Ω, FOR CONICAL SHELLS TESTED (Cont'd)

n \ m	1		2		3	4
	Theo	Exper	Theo	Exper	Exper	Exper
	Shell Model No. 2 (α = 30.2°) (Cont'd)					
18	0.188	0.181	0.270	0.248	0.315	
19		0.195			0.332	0.397
20		0.211		0.280	0.348	
21		0.228		0.297	0.365	
22	0.262	0.244	0.372	0.316	0.384	
23		0.264				
24		0.282		0.356		
25		0.302		0.378		
26	0.344	0.323	0.459	0.402		
27		0.345				
28		0.368				
29		0.391				
30		0.415				
	Shell Model No. 3 (α = 45.1°)					
4	0.324		0.628			
5						
6	0.186	0.164	0.458			
7		0.137				
8	0.128	0.120	0.333			
9		0.112		0.254		
10	0.108	0.108	0.259	0.230		
11		0.110		0.213		
12	0.119	0.116	0.227	0.210	0.344	
13		0.125		0.214	0.319	
14	0.138	0.133	0.229	0.225	0.307	
15		0.143		0.236	0.309	0.380
16	0.158	0.153	0.250		0.322	
17		0.163		0.255	0.334	
18	0.179	0.176	0.265	0.266	0.350	
19		0.188		0.281	0.362	
20		0.201		0.293	0.375	
21		0.217			0.389	
22		0.232		0.319		

TABLE 2. THEORETICAL AND EXPERIMENTAL NATURAL FREQUENCIES, Ω, FOR CONICAL SHELLS TESTED (Cont'd)

n \ m	1		2		3	4
	Theo	Exper	Theo	Exper	Exper	Exper
	Shell Model No. 3 (α = 45.1°) (Cont'd)					
23		0.246		0.332		
24	0.278	0.261	0.378	0.348		
25		0.278		0.358		
26		0.290				
27		0.307				
28		0.323				
29		0.341				
	Shell Model No. 4 (α = 60.5°)					
6	0.179	0.161	0.392			
7		0.134				
8	0.126	0.119	0.306	0.258		
9		0.109		0.227		
10	0.109	0.104	0.249			
11		0.106				
12	0.110	0.108	0.221	0.188		
13		0.112		0.193		
14	0.123	0.121	0.211	0.192		
15		0.128		0.202		
16	0.150		0.237	0.211	0.285	
17		0.146		0.221	0.299	
18		0.158		0.233		
19		0.170		0.244		
20	0.201	0.186	0.292	0.259	0.335	
21		0.200		0.277		
22		0.214		0.296	0.366	
23		0.229		0.314		
24	0.267	0.245	0.377			
25		0.265		0.356		
26		0.282				
27		0.302				
28	0.340	0.324	0.455			
29		0.342				

other freely-supported. These two differ only with respect to the meridional restraint on the displacement u as previously discussed. The effect of relaxing this in-plane constraint is quite pronounced, with the freely-supported condition giving obviously better agreement with experiment. It is this boundary condition that is used for correlation with the other shell models. Although, the effect of the circumferential restraint at the boundary is expected to be less significant, for low values of n it may also have some influence, since, for these modes, the spacing between the nodal points on the boundary is greater, thereby allowing greater circumferential displacements. The imposed circumferential restraint may partially account for the theoretical frequencies being high at low values of n.

Truncation of the series expressions for the mode shapes is also a serious source of error, particularly at large values of n where the mode shapes become highly skewed toward the large end of the cone, as will be shown later. Increasing the number of terms in the series was always found to improve the accuracy. As mentioned earlier, some judgement is required to select the optimum relative number of terms in each series to obtain maximum accuracy for a given size matrix. This selection may change as the parameters of the problem are varied, thereby affecting the relative influence of the respective displacement or stress components.

The frequency plots for the supported conical shells are characterized by having a minimum frequency for each axial mode number m, occurring

at some value of n. This is similar to the behavior of the supported circular cylindrical shell. The value of n at which the minimum frequency occurs is dependent upon the other parameters of the shell, α, s_2/s_1, h/a and ν. For low values of n, the frequency curve turns sharply upward because of the increasing influence of the membrane stiffness in this region. For large n (short wavelength), the stiffness is contributed predominantly by the bending stiffness of the shell.

We might point out again a fact which is obvious from examining the frequency plots, that the density of resonant frequencies is very high. This often results in difficulty in experimental separation of some neighboring modes. Also, the amplitude response at resonance does not appear to have any uniform progression with frequency or mode number. This last factor must be tempered by consideration of the distribution and position of the forcing function as well as possible nonuniform damping of the various modes.

It is difficult to make general statements about the frequency spectrum for freely supported conical shells, since it is influenced by all six independent parameters in (16). In order to get some picture of the influence of cone angle α on the frequency parameter, the theoretical curves in Figure 8 were constructed. At the extreme angles of 0° and 90°, Ω increases regularly with n, while at intermediate angles the relationships between Ω and n is more complicated. For the particular parameters chosen for this

plot ($h/a = 0.01$, $s_2/s_1 = 2.25$, $\nu = 0.30$), the minimum frequency always occurs for $n \leqslant 5$. Also, the stiffest shell in transverse vibration appears to be in the neighborhood of $\alpha = 50°$.

Since for small values of α, the conical shells should behave like circular cylindrical shells, it would be interesting to compare Figure 8 with the similar results given by Arnold and Warburton for thin-wall cylinders (Fig. 2, Ref. 14). It may be noted that the frequency spectrum of cones near $\alpha = 0°$ in Figure 8 is strikingly analogous to that of cylinders near $\lambda = m\pi a/\ell = 0$ in Figure 2, Ref. 14, where ℓ is the total length of the cylinder. It is easy to show that, for small α, the wavelength factor λ is proportional to cone angle α:

$$\lambda \approx \frac{\pi a}{s_2 - s_1} \approx \frac{\pi}{1 - s_1/s_2}\,\alpha$$

In the case under consideration, $s_1/s_2 = 0.444$, therefore, $\lambda = 5.65\alpha$ (α in radian). The values of Ω at $\alpha = 0$ and $\lambda = 0$ agree closely, since both represent the limiting case of an infinite cylinder with $h/a = 0.010$. However, the frequency curves for the cone ascend faster than corresponding curves for the cylinder. This is to be expected as an apparent consequence of the increased stiffness of the conical shell even if it is only slightly tapered.

A decrease in the thickness parameter h/a generally lowers the resonant frequencies because of decreased stiffness, and shifts the minimum frequency to larger values of n, which indicates a change of relative

influence of bending stresses and membrane stresses. For h/a on the order of 0.001 as for the shells tested, the minimum frequency occurs at $n \leqslant 11$ while in the example of Figure 8, h/a = .01, the minimum frequency occurs at $n \leqslant 5$. This is due to the fact that bending stiffness increases as $(h/a)^3$ while the membrane stiffness is proportional only to (h/a).

Mode Shapes

Both experimental and theoretical normalized axial mode shapes are plotted in Figures 9 through 13 for various modes and all four shell models. The theoretical modes are in most cases obtained with a 5 to 7 term truncation of the Fourier series for the normal displacement w. In general, good agreement is obtained. The circumferential mode shapes are, of course, proportional to sin $n\theta$. The nodal pattern for all the modes observed always consisted of parallel circles and equispaced meridians as predicted by the theory.

The most striking feature of the axial mode shape is its strong dependence on the circumferential wave number n for a given shell geometry. This is illustrated in Figures 9, 10, 11, and 13 for m = 1 and in Figures 9 and 12 for m = 2. In each case, the position of maximum displacement or antinode shifts toward the large diameter of the shell, $s = s_2$, with increasing circumferential wave number n. For low values of n and in the neighborhood of the minimum frequency, the displacement

is relatively symmetric and therefore can be described with a fewer number of terms in the Fourier series. This is the region where the best agreement is obtained for the resonant frequencies. At large values of n, the displacement becomes highly skewed toward the large end of the cone, with little transverse motion occurring at the small end. Obviously, to achieve good agreement in this region, for either mode shape or resonant frequency, will require retaining additional terms in the series, not only for the normal displacement w, but also for the other displacement or stress components. Physically, the suppression of normal displacement near the small end of the cone at large values of n is due to high stiffness and the short distance between consecutive nodal meridians in this region, i.e., there are 2n points of zero normal displacement around a circumference. The displacements between these nodal lines are therefore necessarily smaller near the minor end. The curvatures and stresses in this region, however, are not necessarily small.

The geometry of the shell also has an effect on the normalized mode shapes. For comparison, the same mode, n = 8, m = 1, is plotted in Figures 9, 10, 11a and 13 for the four shell models. It is interesting to note that for this mode the theoretical mode shape for $\alpha = 14.2°$ is skewed toward the large end, $s = s_2$, while for the other three shells, $\alpha = 30.2°$, $45.1°$, $60.5°$, the theoretical mode shapes are skewed toward the small end, $s = s_1$. This seems dependent on whether the circumferential wave number n = 8 being larger or smaller than the wave number at which the

minimum resonant frequency occurs, and therefore whether the bending or membrane stresses are more influential. The experimental results for this mode are not as consistent on this point, particularly for $\alpha = 60.5°$. The general observation appears to be valid, however. For instance, in Figure 9 for $\alpha = 14.2°$, the mode $n = 8$, $m = 1$ is skewed towards $s = s_2$, and the mode $n = 8$, $m = 2$ is skewed towards $s = s_1$. The former is on the bending portion of the Ω vs n curve while the latter is at the minimum of the curve and more strongly affected by the membrane effects.

A few more comments are appropriate with regard to the theoretical and experimental mode shapes. The negative deflections indicated for some of the theoretical mode shapes for $m = 1$ are a result of the limited number of terms in the series expression for w and should not imply the existence of an additional nodal circle. In addition, the experimental displacement curve is generally shifted to the right with respect to the theoretical curve, perhaps due to the experimental boundary condition which held the small end of the cone more tightly than the large end.

CONCLUSIONS

It is felt that the following conclusions may be justifiably made from work presented.

1. The analytical procedure used is adequate to predict the resonant frequencies and mode shapes for transverse vibration of truncated conical shells over a wide range in the geometrical, material and modal parameters. The numerical procedure is particularly efficient for shells with homogeneous boundary conditions, where, as in the example presented, each submatrix of the coefficient matrix are generated by a single close-form algebraic expression. While still applicable to nonhomogeneous boundary conditions, much of the computational efficiency of the method may be lost because a rather complicated form of series expansion has to be employed to represent the mode functions, and an appropriate transformation [such as the one which transforms (1) into (9) or (13) used herein] must be applied.

2. The accuracy of the analytical results is strongly dependent upon the degree of satisfaction of the boundary conditions and the number of terms retained in the series expansion of each of the mode functions, the latter being particularly significant for the higher modes.

3. The order of occurrence of the resonant frequencies in terms of the modal parameters m and n is strongly dependent on the geometry of the shell.

4. For the shell supported at both edges, a minimum resonant frequency for each m value occurs, which separates that branch of the frequency spectrum predominantly associated with membrane effects from that associated with bending stiffness.

5. The modal shape in the meridional direction is strongly dependent on the circumferential wave number n, with the predominant transverse motion shifting toward the larger end of the cone as n increases.

ACKNOWLEDGEMENTS

The authors wish to gratefully acknowledge Messrs. T. Jackson and R. Gonzales for their assistance in the computer program, Mr. D. Kana for his assistance in performing the experiments and Messrs. J. Gormley and V. Hernandez for preparation of the figures.

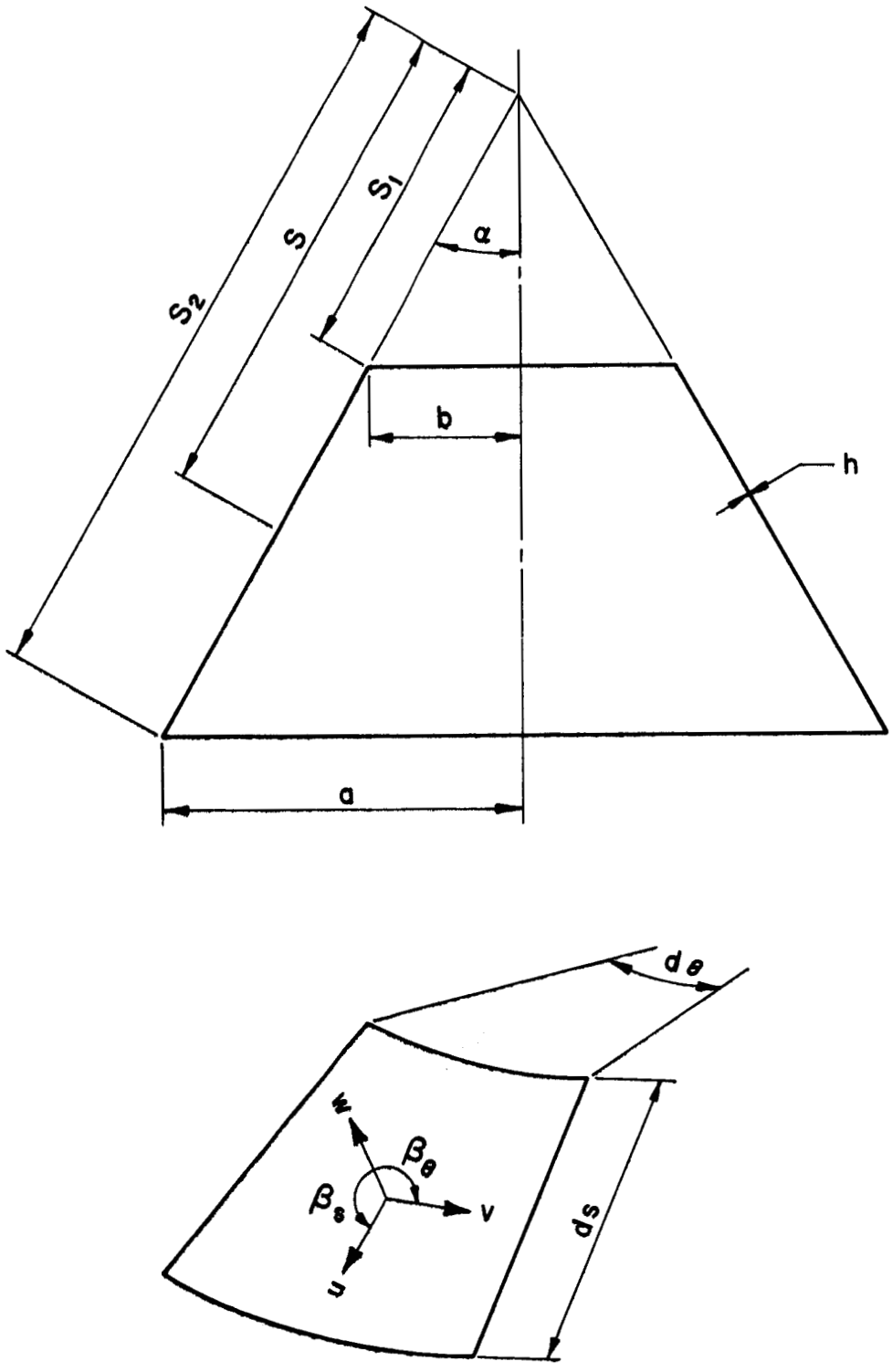

FIGURE 1. SHELL GEOMETRY AND COORDINATE SYSTEM

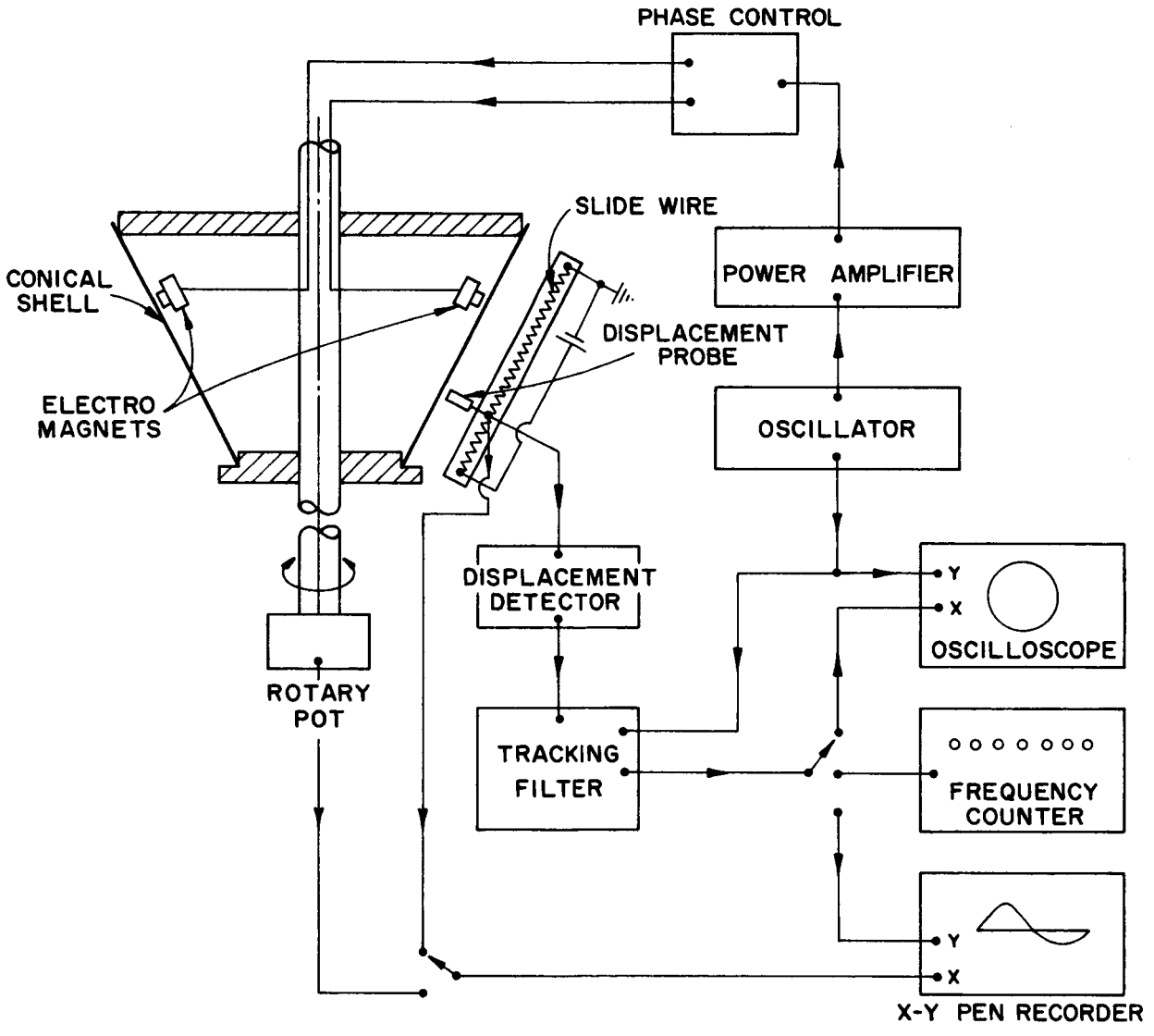

FIGURE 2. SCHEMATIC OF EXPERIMENTAL APPARATUS

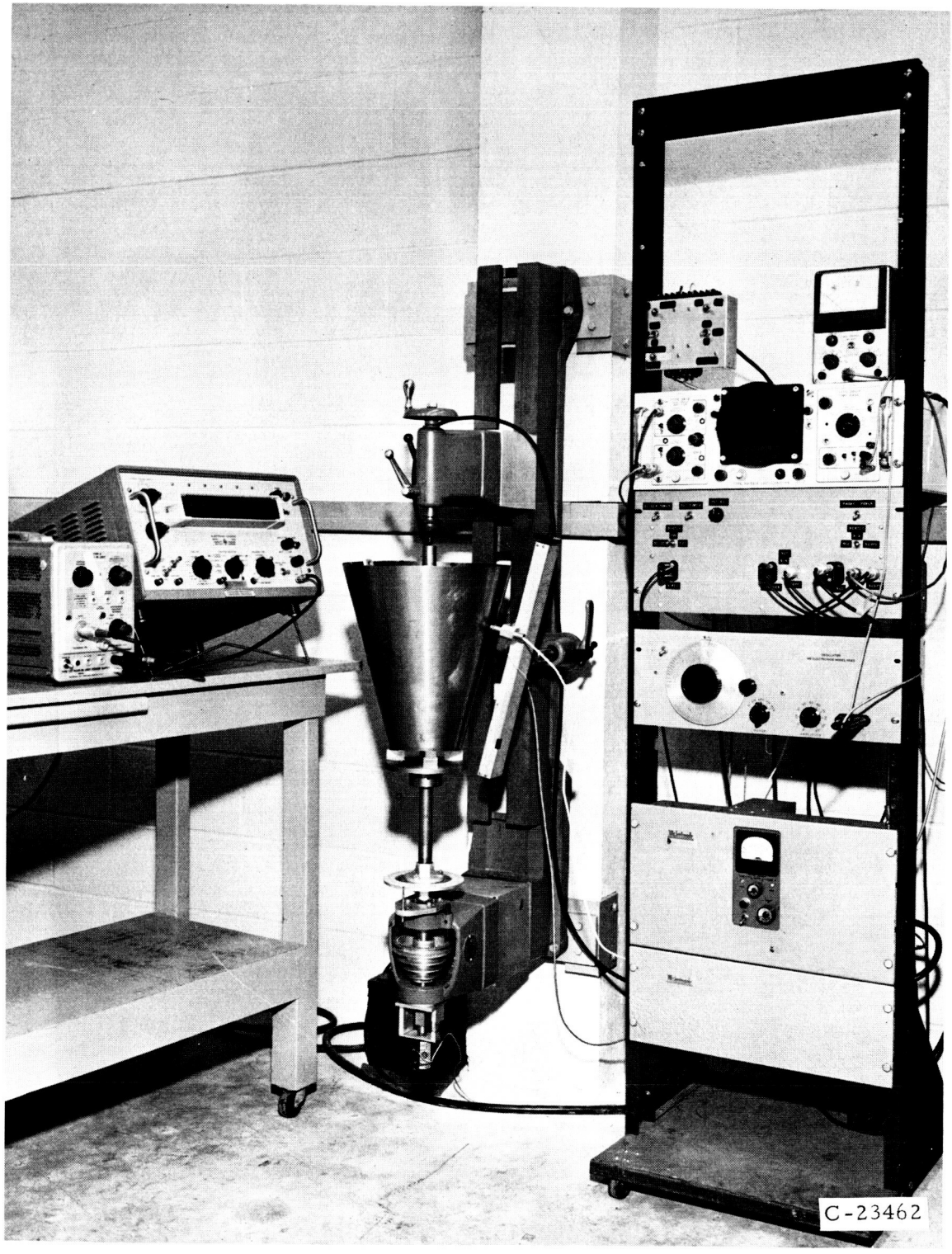

FIGURE 3. PHOTOGRAPH OF EXPERIMENTAL SETUP

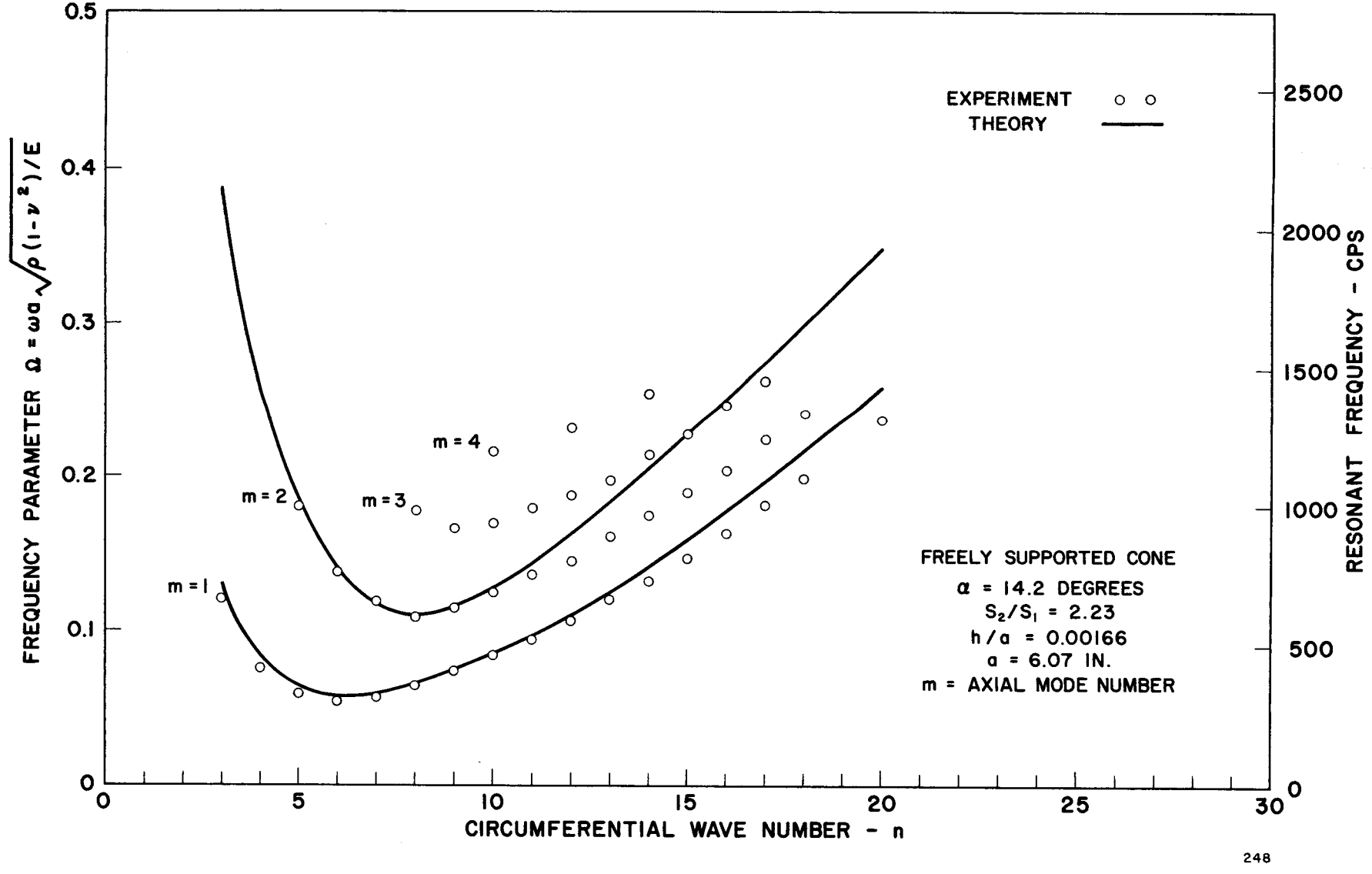

FIGURE 4. THEORETICAL AND EXPERIMENTAL FREQUENCY VS CIRCUMFERENTIAL WAVE NUMBER FOR 14.2° CONICAL SHELL

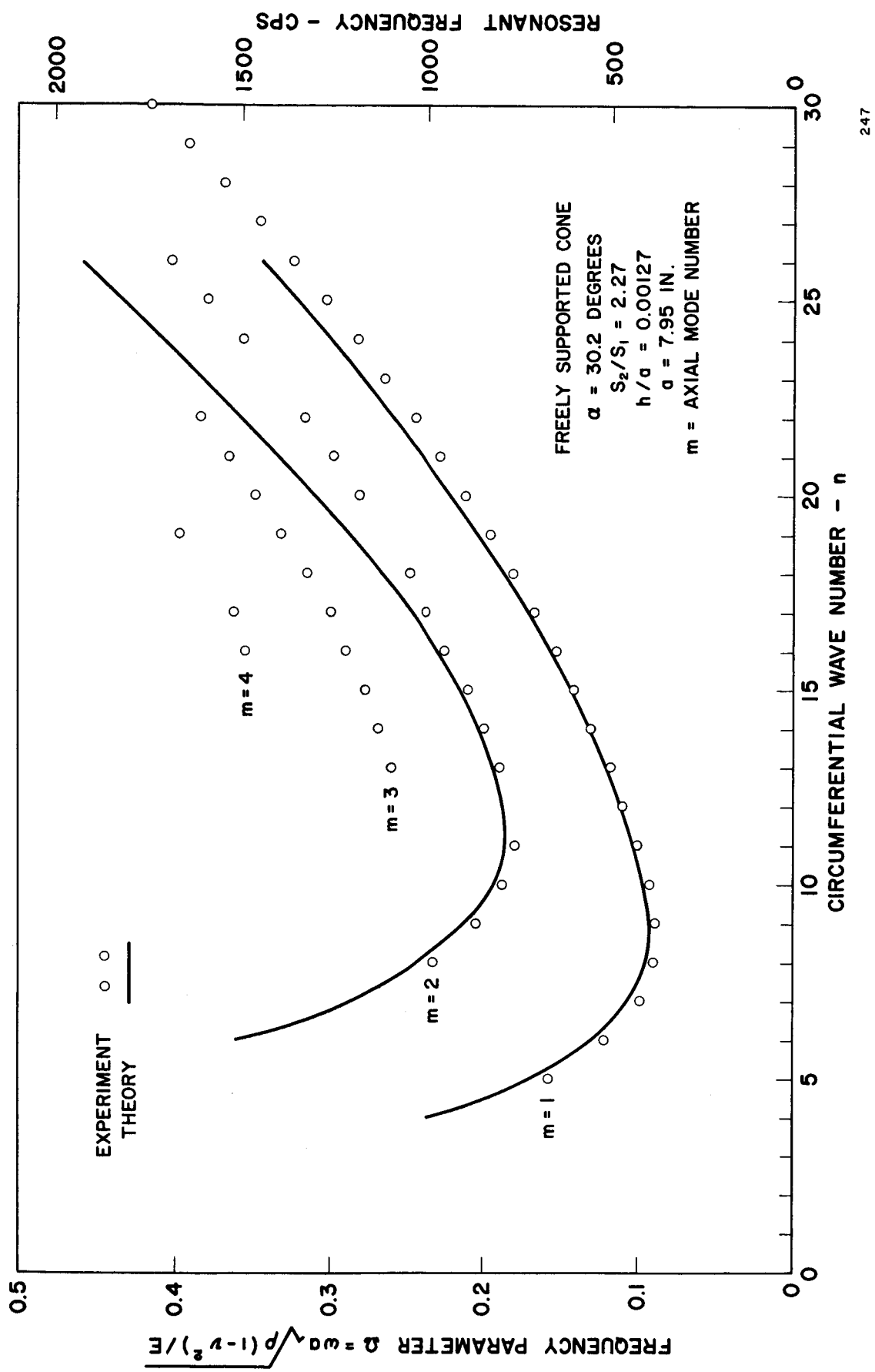

FIGURE 5. THEORETICAL AND EXPERIMENTAL FREQUENCY VS CIRCUMFERENTIAL WAVE NUMBER FOR 30.2° CONE

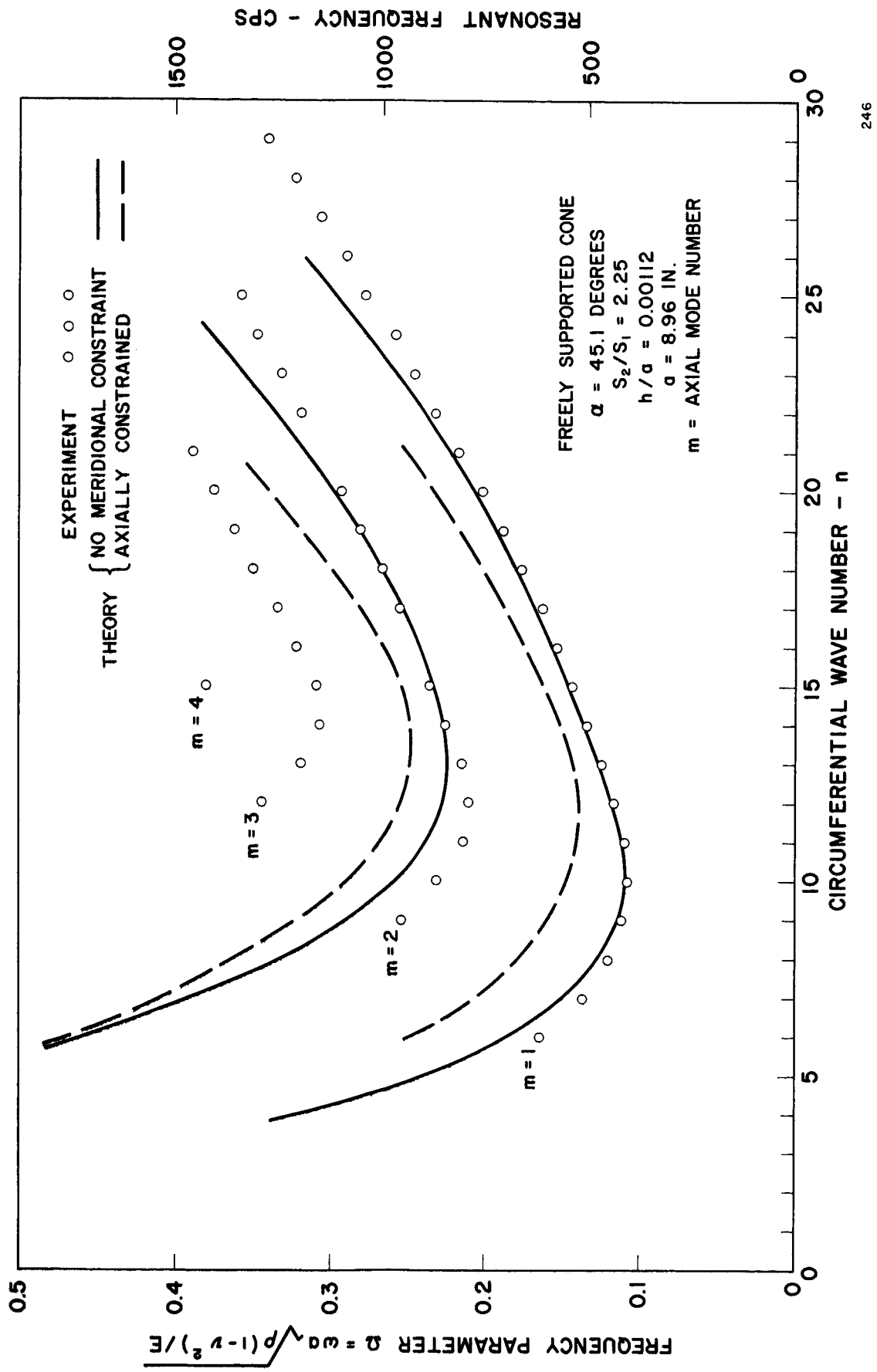

FIGURE 6. THEORETICAL AND EXPERIMENTAL FREQUENCY VS CIRCUMFERENTIAL WAVE NUMBER FOR 45.1° CONE

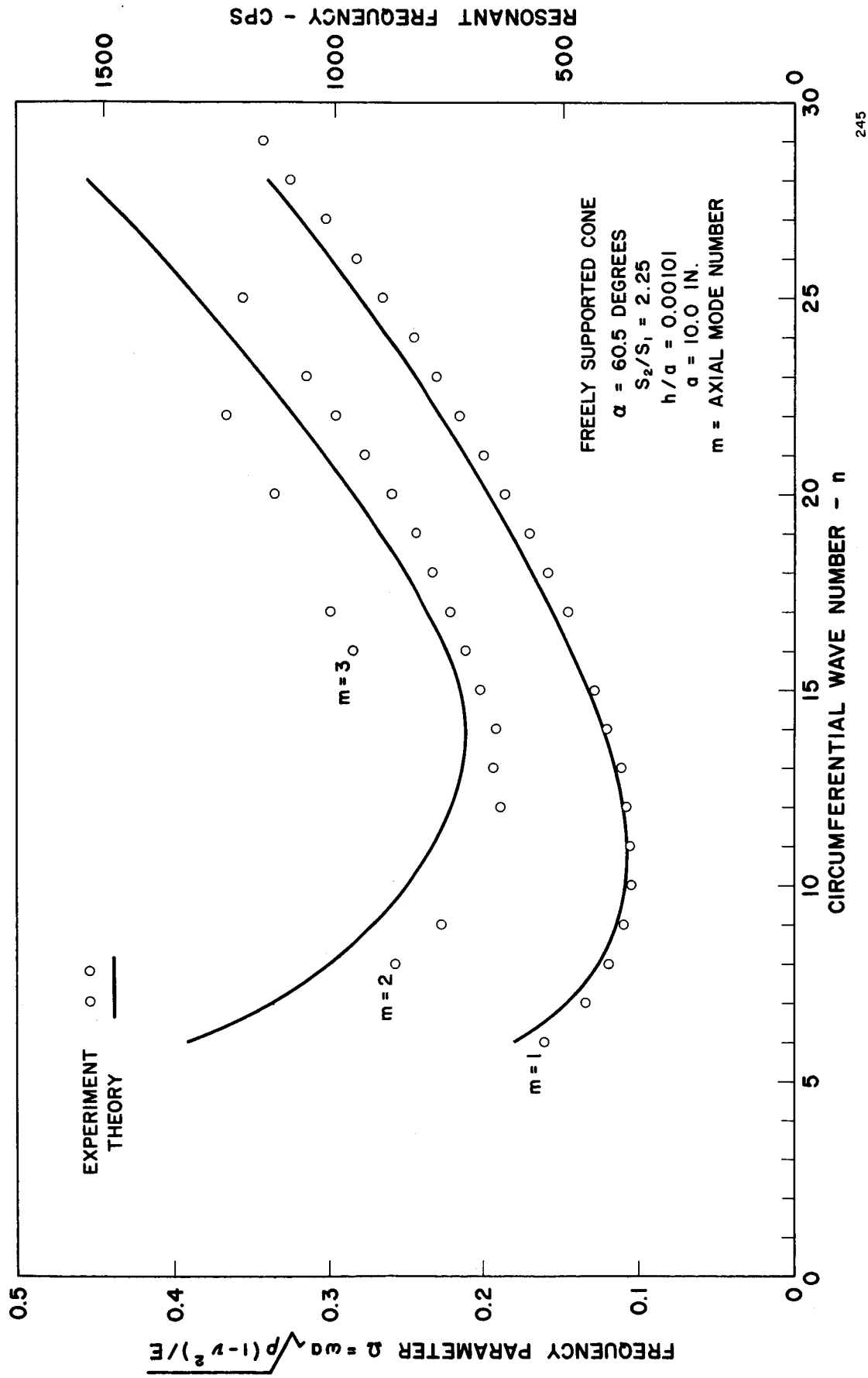

FIGURE 7. THEORETICAL AND EXPERIMENTAL FREQUENCY VS CIRCUMFERENTIAL WAVE NUMBER FOR 60.5° CONE

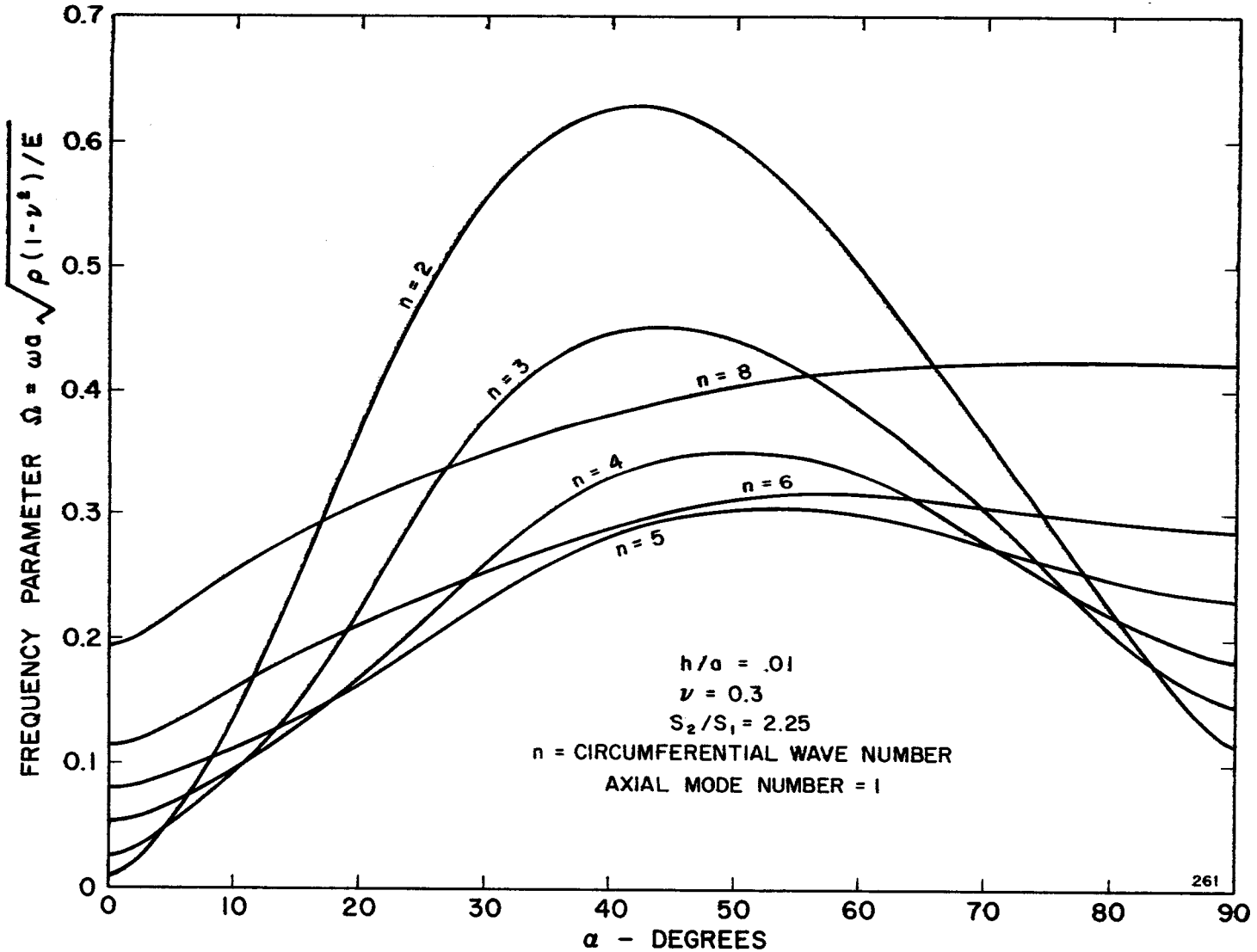

FIGURE 8. THEORETICAL FREQUENCY VS CONE ANGLE FOR VARIOUS VALUES OF CIRCUMFERENTIAL WAVE NUMBER

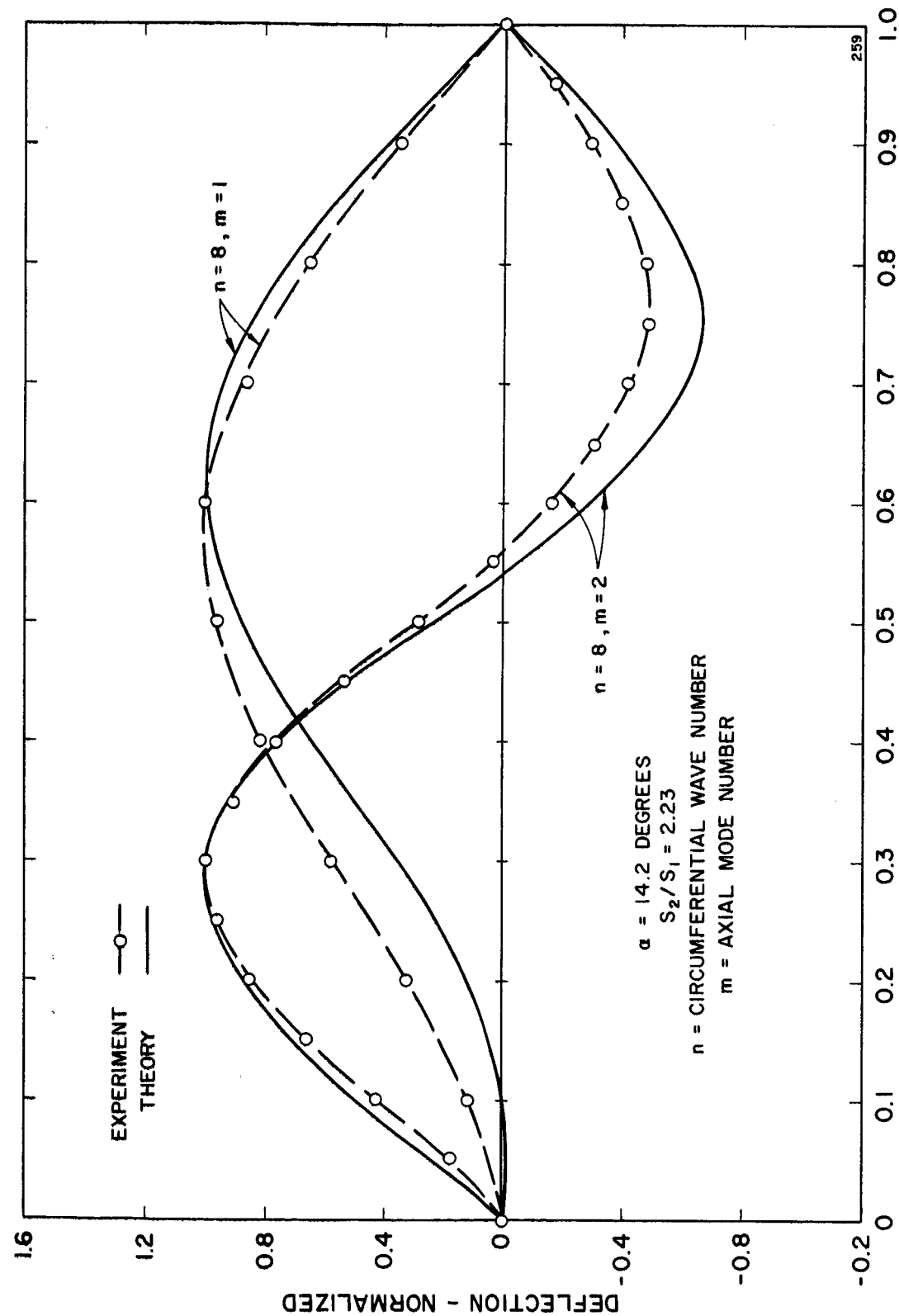

FIGURE 9. THEORETICAL AND EXPERIMENTAL TRANSVERSE MODE SHAPES FOR FREELY SUPPORTED 14.2° CONE

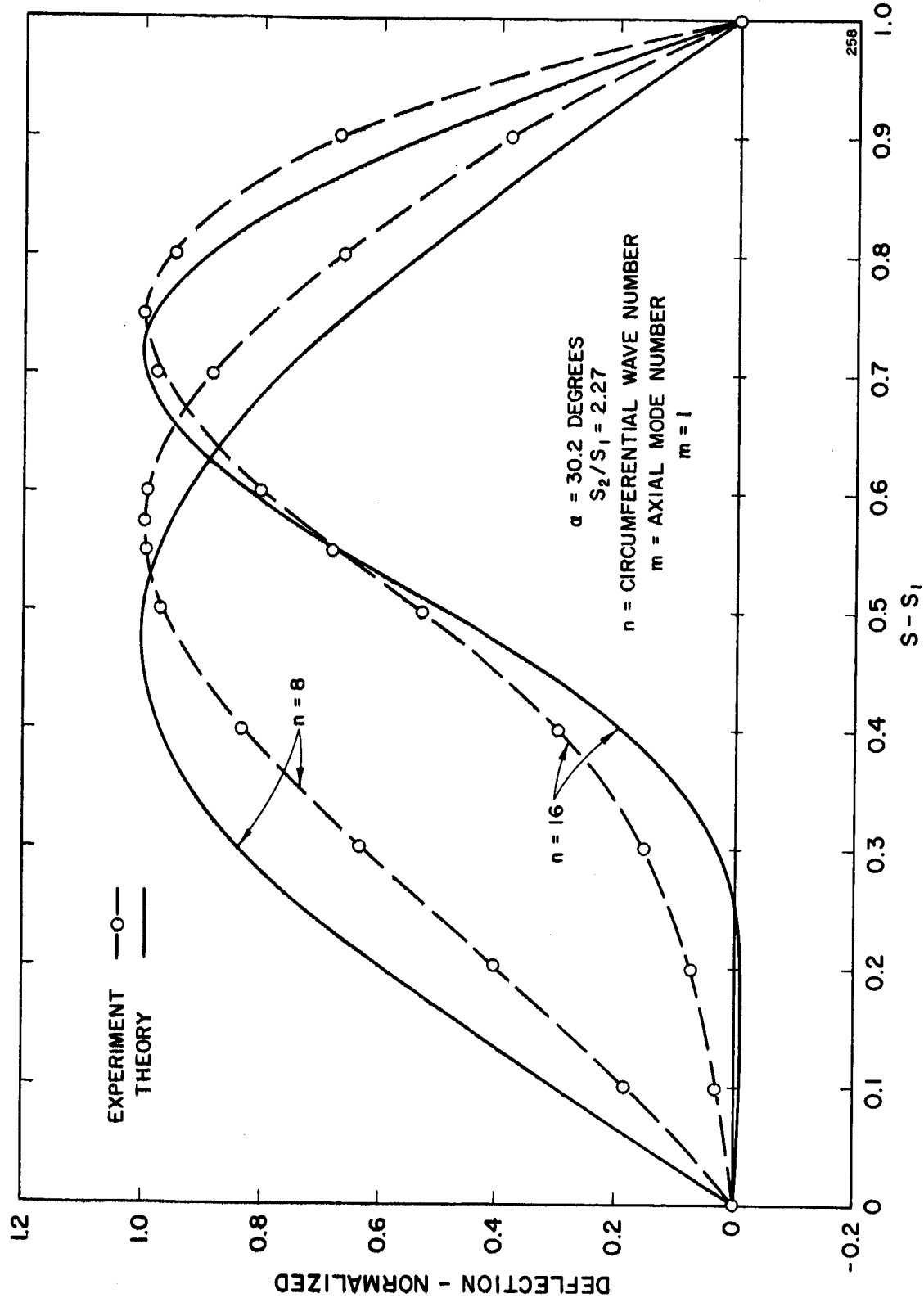

FIGURE 10. THEORETICAL AND EXPERIMENTAL TRANSVERSE MODE SHAPES FOR FREELY SUPPORTED 30.2° CONE

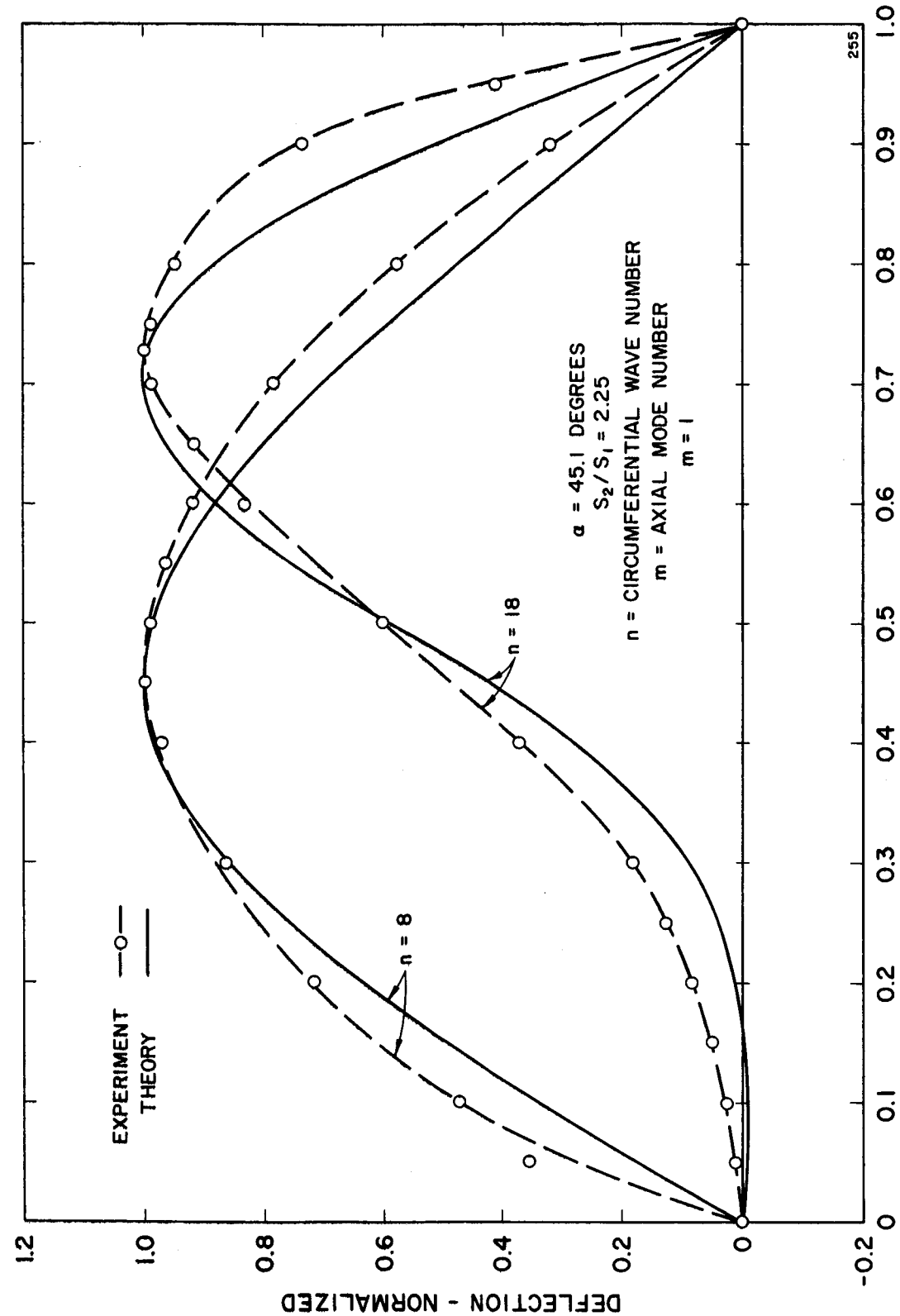

FIGURE 11a. THEORETICAL AND EXPERIMENTAL TRANSVERSE MODE SHAPES FOR FREELY SUPPORTED 45.1° CONE

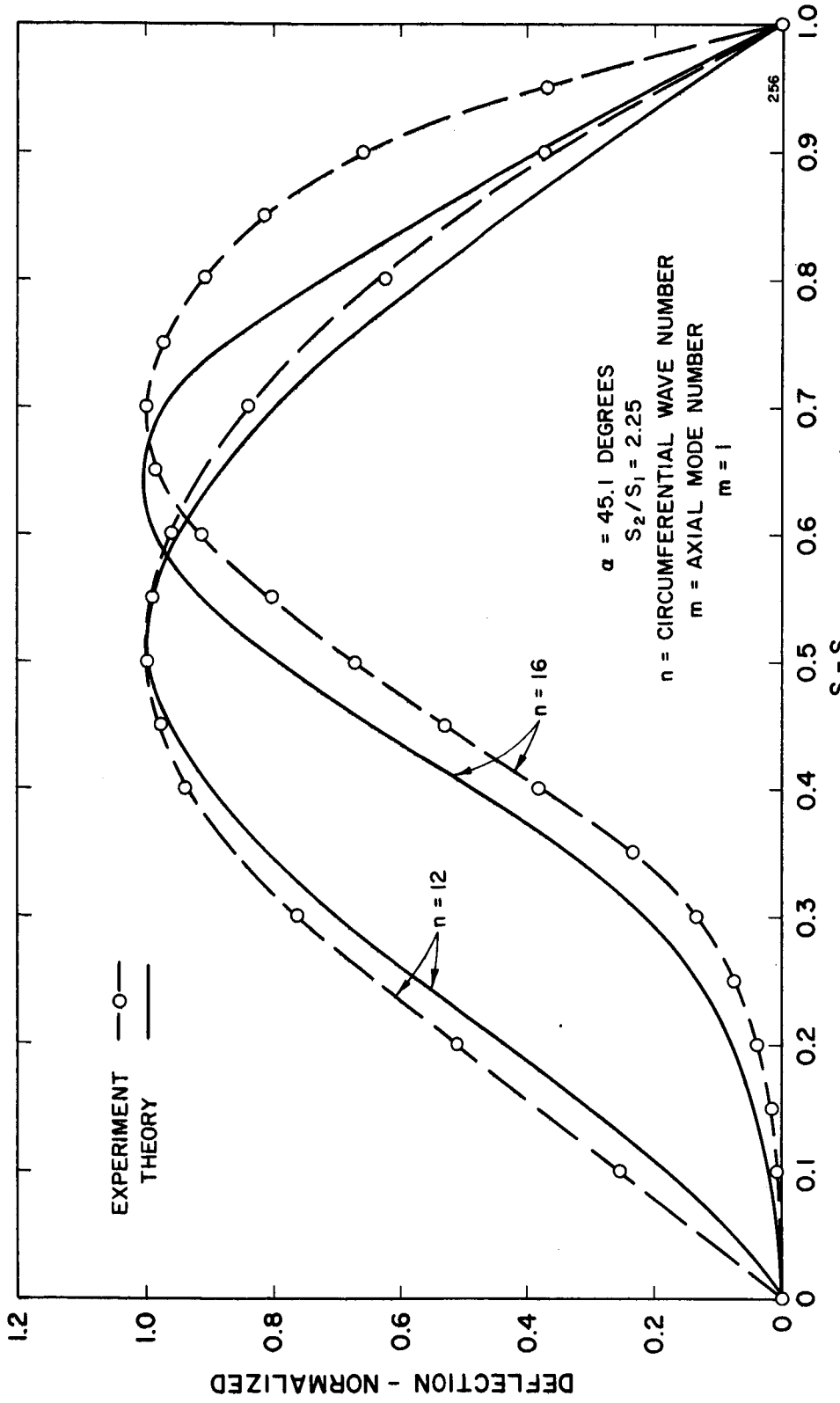

FIGURE 11b. THEORETICAL AND EXPERIMENTAL TRANSVERSE MODE SHAPES FOR FREELY SUPPORTED 45.1° CONE

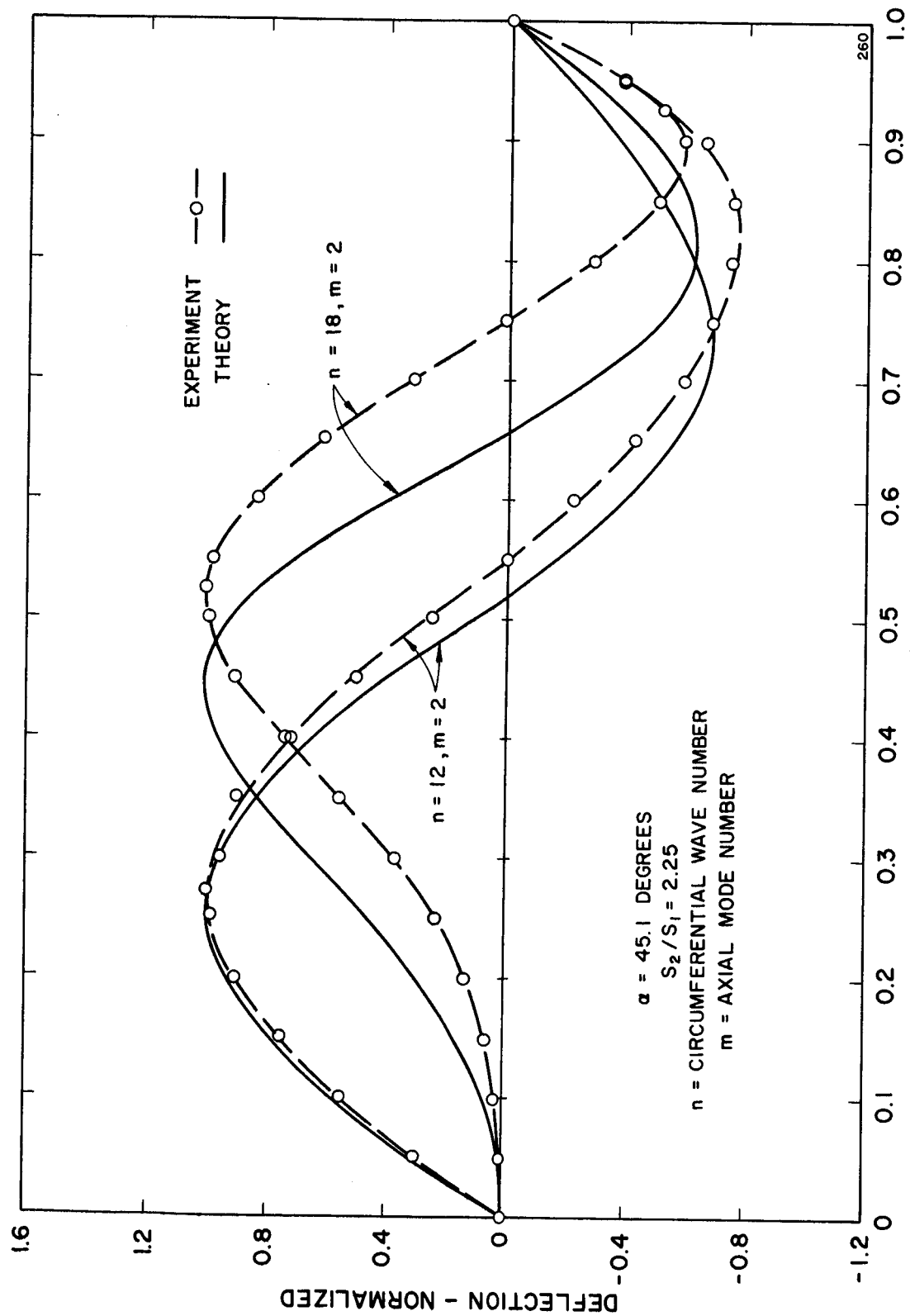

FIGURE 12. THEORETICAL AND EXPERIMENTAL SHAPE OF SECOND AXIAL MODE OF FREELY SUPPORTED 45.1° CONE

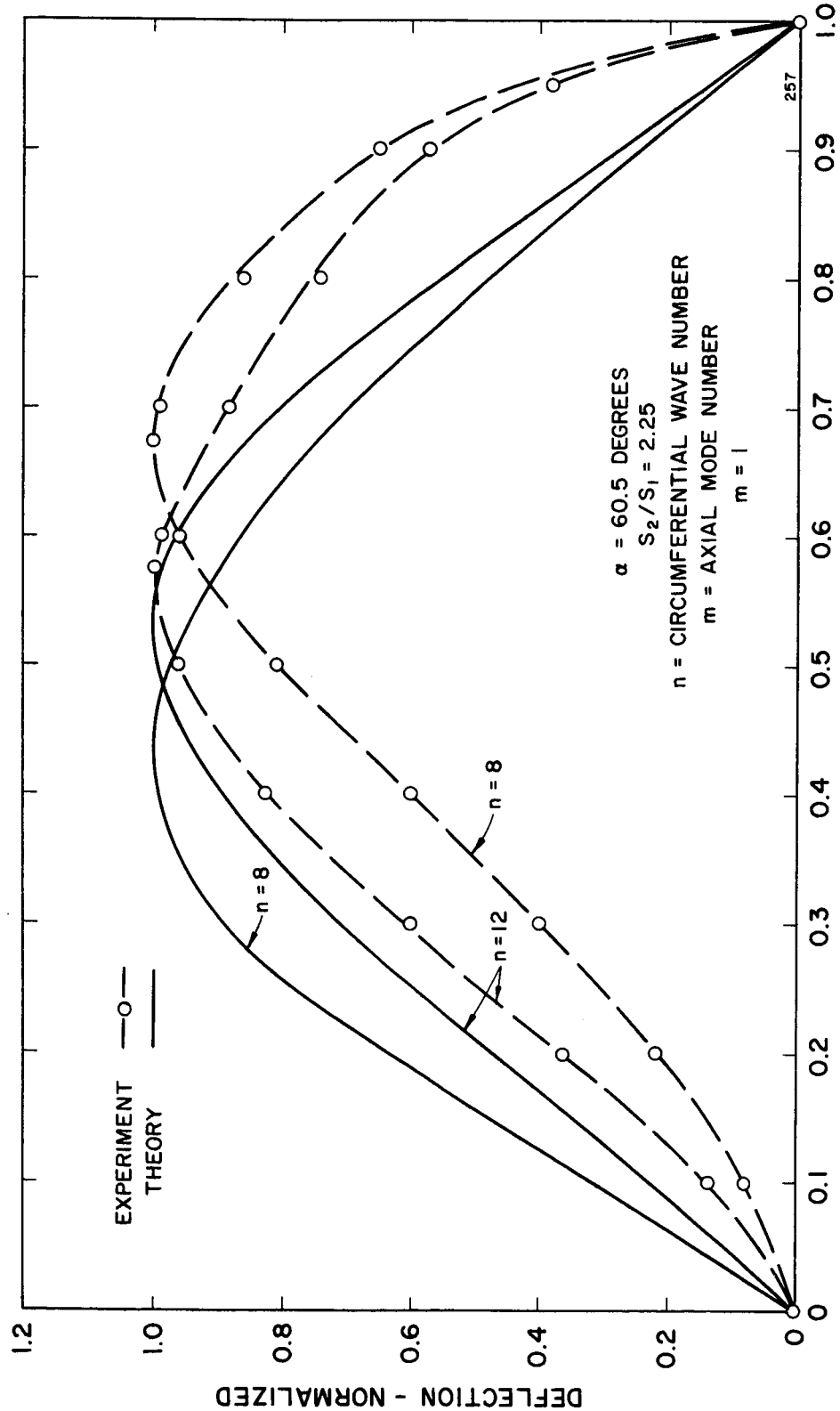

FIGURE 13. THEORETICAL AND EXPERIMENTAL TRANSVERSE MODE SHAPE FOR FREELY SUPPORTED 60.5° CONE

APPENDIX I

The elements of the operator matrix H^*

$$H^{*11} = e^{2x}\left[-\sin^2\alpha\,(\mathcal{D}^2 - 1) + \frac{1-\nu}{2}n^2\right]$$

$$H^{*12} = -n\sin\alpha\, e^{2x}\left[\frac{1+\nu}{2}\mathcal{D} + \frac{3-\nu}{2}\right]$$

$$H^{*13} = \sin\alpha\cos\alpha\, e^{2x}(\nu\mathcal{D} + 1)$$

$$H^{*14} = 0$$

$$H^{*21} = n\sin\alpha\, e^{2x}\left[\frac{1+\nu}{2}\mathcal{D} - \frac{3-\nu}{2}\right]$$

$$H^{*22} = e^{2x}\left[-\frac{1-\nu}{2}\sin^2\alpha\,(\mathcal{D}^2 - 1) + n^2\right]$$

$$H^{*23} = -n\cos\alpha\, e^{2x} + \epsilon n\cos\alpha\, e^{4x}\left[\frac{1-\nu}{2}\sin^2\alpha\,(\mathcal{D}^2 + 2\mathcal{D}) - n^2\right]$$

$$H^{*24} = \epsilon n\sin\alpha\cos\alpha\, e^{3x}\left[\frac{1+\nu}{2}\mathcal{D} - \frac{3-\nu}{2}\right]$$

$$H^{*31} = -\sin\alpha\cos\alpha\, e^{2x}[\nu\mathcal{D} - 1]$$

$$H^{*32} = -n\cos\alpha\, e^{2x}$$

$$H^{*33} = e^{2x}[-k_s\sin^2\alpha\,\mathcal{D}^2 + \cos^2\alpha] - \epsilon n^2 e^{4x}\left[\frac{1-\nu}{2}\sin^2\alpha\,(\mathcal{D}^2 + 2\mathcal{D}) - n^2\right]$$

$$H^{*34} = k_s\sin\alpha\, e^{x}(\mathcal{D} - 1) - \epsilon n^2\sin\alpha\, e^{3x}\left[\frac{1+\nu}{2}\mathcal{D} - \frac{3-\nu}{2}\right]$$

$$H^{*41} = 0$$

$$H^{*42} = 0$$

$$H^{*43} = -(k_s/\epsilon)\sin\alpha\, e^{x}\mathcal{D} + n^2\sin\alpha\, e^{3x}\left[\frac{1+\nu}{2}\mathcal{D} + 2\right]$$

$$H^{*44} = e^{2x}\left[-\sin^2\alpha\,(\mathcal{D}^2 - 1) + \frac{1-\nu}{2}n^2\right] + (k_s/\epsilon)$$

where $\mathcal{D} = d/d_x$ is the differential operator.

APPENDIX II

Let k and m be positive integers or zero, and γ be any positive real number. Define

$$P_{km}^{(\gamma)} = \frac{2}{L}\int_0^L e^{\gamma x}\sin\frac{k\pi x}{L}\sin\frac{m\pi x}{L}\,dx$$

$$= \left[\frac{\gamma L}{\gamma^2 L^2+(k-m)^2\pi^2} - \frac{\gamma L}{\gamma^2 L^2+(k+m)^2\pi^2}\right]\left[(-1)^{k+m}e^{\gamma L}-1\right]$$

$$Q_{km}^{(\gamma)} = \frac{2}{L}\int_0^L e^{\gamma x}\sin\frac{k\pi x}{L}\cos\frac{m\pi x}{L}\,dx$$

$$= -\left[\frac{(k-m)\pi}{\gamma^2 L^2+(k-m)^2\pi^2} + \frac{(k+m)\pi}{\gamma^2 L^2+(k+m)^2\pi^2}\right]\left[(-1)^{k+m}e^{\gamma L}-1\right]$$

$$R_{km}^{(\gamma)} = \frac{2}{L}\int_0^L e^{\gamma x}\cos\frac{k\pi x}{L}\cos\frac{m\pi x}{L}\,dx$$

$$= \left[\frac{\gamma L}{\gamma^2 L^2+(k-m)^2\pi^2} + \frac{\gamma L}{\gamma^2 L^2+(k+m)^2\pi^2}\right]\left[(-1)^{k+m}e^{\gamma L}-1\right]$$

When $\gamma = 0$, and $k = m$, the above formulas are indeterminate. The integrals can be easily evaluated as following

$$P_{kk}^{(0)} = 1\ ,\quad Q_{kk}^{(0)} = 0\ ,\quad R_{kk}^{(0)} = 1\ ,\quad P_{00}^{(0)} = 0,\quad R_{00}^{(0)} = 2$$

Denote $\mu = \frac{m\pi}{L}$

The coefficients A_{km}^{ij} for simply supported edges with axial constraint are:

$$A^{11}_{km} = \left[\sin^2\alpha\,(\mu^2+1) + \frac{1-\nu}{2}n^2\right]P^{(2)}_{km} \qquad m=1 \sim M_1$$

$$A^{12}_{km} = -n\sin\alpha\left[\frac{1+\nu}{2}\mu\,Q^{(2)}_{km} + \frac{3-\nu}{2}P^{(2)}_{km}\right] \qquad m=1 \sim M_2$$

$$A^{13}_{km} = \sin\alpha\cos\alpha\left[\nu\mu\,Q^{(2)}_{km} + P^{(2)}_{km}\right] \qquad m=1 \sim M_3$$

$$A^{14}_{km} = 0 \qquad m=0 \sim M_4$$

$k = 1 \sim M_1$

$$A^{21}_{km} = n\sin\alpha\left[\frac{1+\nu}{2}\mu Q^{(2)}_{km} - \frac{3-\nu}{2}P^{(2)}_{km}\right] \qquad m=1 \sim M_1$$

$$A^{22}_{km} = \left[\frac{1-\nu}{2}\sin^2\alpha\,(\mu^2+1) + n^2\right]P^{(2)}_{km} \qquad m=1 \sim M_2$$

$$A^{23}_{km} = -n\cos\alpha\,P^{(2)}_{km} - \epsilon n\cos\alpha\left[\left(\frac{1-\nu}{2}\mu^2\sin^2\alpha + n^2\right)P^{(4)}_{km} - (1-\nu)\mu\sin^2\alpha\,Q^{(4)}_{km}\right] \qquad m=1 \sim M_3$$

$$A^{24}_{ko} = -\epsilon n\sin\alpha\cos\alpha\left(\frac{3-2\nu-\nu^2}{4}\right)Q^{(3+\nu)}_{ko} \qquad (m=0)$$

$$A^{24}_{km} = -\epsilon n\sin\alpha\cos\alpha\left[\frac{1+\nu}{2}\mu P^{(3+\nu)}_{km} + \frac{3-2\nu-\nu^2}{2}Q^{(3+\nu)}_{km}\right] \qquad m=1 \sim M_4$$

$k = 1 \sim M_2$

$$A^{31}_{km} = -\sin\alpha\cos\alpha\left[\nu\mu Q^{(2)}_{km} - P^{(2)}_{km}\right] \qquad m=1 \sim M_1$$

$$A^{32}_{km} = -n\cos\alpha\,P^{(2)}_{km} \qquad m=1 \sim M_2$$

$$A^{33}_{km} = (k_s\mu^2\sin^2\alpha + \cos^2\alpha)\,P^{(2)}_{km} + \epsilon n^2\left[\left(\frac{1-\nu}{2}\mu^2\sin^2\alpha + n^2\right)P^{(4)}_{km} - (1-\nu)\mu\sin^2\alpha\,Q^{(4)}_{km}\right] \qquad m=1 \sim M_3$$

$$A^{34}_{ko} = -k_s\sin\alpha\left[\frac{1-\nu}{2}Q^{(1+\nu)}_{ko}\right] + \epsilon n^2\sin\alpha\left[\frac{3-2\nu-\nu^2}{4}Q^{(3+\nu)}_{ko}\right] \qquad (m=0)$$

$$A^{34}_{km} = -k_s\sin\alpha\left[\mu P^{(1+\nu)}_{km} + (1-\nu)Q^{(1+\nu)}_{km}\right] + \epsilon n^2\sin\alpha\left[\frac{1+\nu}{2}\mu P^{(3+\nu)}_{km} + \frac{3-2\nu-\nu^2}{2}Q^{(3+\nu)}_{km}\right] \qquad m=1 \sim M_4$$

$k = 1 \sim M_3$

$$A_{km}^{41} = 0 \qquad m=1 \sim M_1$$

$$A_{km}^{42} = 0 \qquad m=1 \sim M_2$$

$$A_{km}^{43} = -(k_s/\epsilon)\,\mu \sin\alpha\, R_{km}^{(1-\nu)} + n^2 \sin\alpha \left[\frac{1+\nu}{2}\,\mu R_{km}^{(3-\nu)} + 2Q_{mk}^{(3-\nu)}\right] \qquad m=1 \sim M_3$$

$$A_{ko}^{44} = \left[\sin^2\alpha\,(1-\nu^2) + \frac{1-\nu}{2}\,n^2\right]\frac{1}{2}\,R_{ko}^{(2)} + (k_s/2\epsilon)\,R_{ko}^{(0)} \qquad (m=0)$$

$$A_{km}^{44} = \left[\sin^2\alpha\,(\mu^2+1-\nu^2) + \frac{1-\nu}{2}\,n^2\right] R_{km}^{(2)} + 2\nu\mu \sin^2\alpha\, Q_{mk}^{(2)} + (k_s/\epsilon)\,R_{km}^{(0)} \qquad m=1 \sim M_4$$

$$k=0 \sim M_4$$

APPENDIX III

The coefficients B^{ij}_{km} for freely supported edges without meridional constraint are

$$B^{11}_{ko} = \left[\sin^2\alpha\,(1-\nu^2) + \frac{1-\nu}{2}\,n^2\right]\,\frac{1}{2}\,R^{(2)}_{ko} \qquad (m=0)$$

$$B^{11}_{km} = \left[\sin^2\alpha\,(\mu^2+1-\nu^2) + \frac{1-\nu}{2}\,n^2\right]\,R^{(2)}_{km} - 2\nu\mu\sin^2\alpha\,Q^{(2)}_{mk} \qquad m=1 \sim M_1$$

$$B^{12}_{km} = -n\sin\alpha\left[\frac{1+\nu}{2}\mu R^{(2-\nu)}_{km} + \frac{3-\nu}{2}\,Q^{(2-\nu)}_{mk}\right] \qquad m=1 \sim M_2$$

$$B^{13}_{km} = \sin\alpha\cos\alpha\left[\nu\mu R^{(2-\nu)}_{km} + Q^{(2-\nu)}_{mk}\right] \qquad m=1 \sim M_3$$

$$B^{14}_{km} = 0 \qquad m=0 \sim M_4$$

$\Big\}\; k = 0 \sim M_1$

$$B^{21}_{ko} = -n\sin\alpha\left[\frac{3-2\nu-\nu^2}{4}\,Q^{(2+\nu)}_{ko}\right] \qquad (m=0)$$

$$B^{21}_{km} = -n\sin\alpha\left[\frac{1+\nu}{2}\,\mu P^{(2+\nu)}_{km} + \frac{3-2\nu-\nu^2}{2}\,Q^{(2+\nu)}_{km}\right] \qquad m=1 \sim M_1$$

$$B^{22}_{km} = \left[\frac{1-\nu}{2}\sin^2\alpha\,(\mu^2+1) + n^2\right]\,P^{(2)}_{km} \qquad m=1 \sim M_2$$

$$B^{23}_{km} = -n\cos\alpha\,P^{(2)}_{km} - \epsilon n\cos\alpha\left[\left(\frac{1-\nu}{2}\,\mu^2\sin^2\alpha + n^2\right)\,P^{(4)}_{km} - (1-\nu)\,\mu\sin^2\alpha\,Q^{(4)}_{km}\right] \qquad m=1 \sim M_3$$

$$B^{24}_{ko} = -\epsilon n\sin\alpha\cos\alpha\left[\frac{3-2\nu-\nu^2}{4}\,Q^{(3+\nu)}_{ko}\right] \qquad (m=0)$$

$$B^{24}_{km} = -\epsilon n\sin\alpha\cos\alpha\left[\frac{1+\nu}{2}\,\mu P^{(3+\nu)}_{km} + \frac{3-2\nu-\nu^2}{2}\,Q^{(3+\nu)}_{km}\right] \qquad m=1 \sim M_4$$

$\Big\}\; k = 1 \sim M_2$

$$B^{31}_{ko} = \sin\alpha\cos\alpha \left[\frac{1-\nu}{2} Q^{(2+\nu)}_{ko}\right] \qquad (m=0)$$

$$B^{31}_{km} = \sin\alpha\cos\alpha \left[\nu\mu P^{(2+\nu)}_{km} + (1-\nu) Q^{(2+\nu)}_{km}\right] \qquad m=1 \sim M_1$$

$$B^{32}_{km} = -n\cos\alpha\, P^{(2)}_{km} \qquad m=1 \sim M_2$$

$$B^{33}_{km} = (k_s\mu^2 \sin^2\alpha + \cos^2\alpha) P^{(2)}_{km} + \epsilon n \left[\left(\frac{1-\nu}{2}\mu^2 \sin^2\alpha + n^2\right) P^{(4)}_{km} - (1-\nu)\mu \sin^2\alpha\, Q^{(4)}_{km}\right] \qquad m=1 \sim M_3$$

$$B^{34}_{ko} = -k_s \sin\alpha \left[\frac{1-\nu}{2} Q^{(1+\nu)}_{ko}\right] + \epsilon n^2 \sin\alpha \left[\frac{3-2\nu-\nu^2}{4} Q^{(3+\nu)}_{ko}\right] \qquad (m=0)$$

$$B^{34}_{km} = -k_s \sin\alpha \left[\mu P^{(1+\nu)}_{km} + (1-\nu) Q^{(1+\nu)}_{km}\right] + \epsilon n^2 \sin\alpha \left[\frac{1+\nu}{2}\mu P^{(3+\nu)}_{km} + \frac{3-2\nu-\nu^2}{2} Q^{(3+\nu)}_{km}\right] \qquad m=1 \sim M_4$$

$k = 1 \sim M_3$

$$B^{41}_{km} = 0 \qquad m=0 \sim M_1$$

$$B^{42}_{km} = 0 \qquad m=1 \sim M_2$$

$$B^{43}_{km} = -(k_s/\epsilon)\mu \sin\alpha\, R^{(1-\nu)}_{km} + n^2 \sin\alpha \left[\frac{1+\nu}{2}\mu R^{(3-\nu)}_{km} + 2Q^{(3-\nu)}_{km}\right] \qquad m=1 \sim M_3$$

$$B^{44}_{ko} = \left[\sin^2\alpha\,(1-\nu^2) + \frac{1-\nu}{2} n^2\right] \frac{1}{2} R^{(2)}_{ko} + (k_s/2\epsilon) R^{(0)}_{ko} \qquad (m=0)$$

$$B^{44}_{km} = \left[\sin^2\alpha\,(\mu^2 + 1 - \nu^2) + \frac{1-\nu}{2} n^2\right] R^{(2)}_{km} + 2\nu\mu \sin^2\alpha\, Q^{(2)}_{mk} + (k_s/\epsilon) R^{(0)}_{km} \qquad m=1 \sim M_4$$

$k = 0 \sim M_4$

REFERENCES

1. Hu, W. C. L., "A Survey of the Literature on the Vibrations of Thin Shells," Tech. Rep. No. 1, Contract No. NASr-94(06), Southwest Research Institute (1964).

2. Hu, W. C. L., "Free Vibrations of Conical Shells," NASA TN D-2666 (1965).

3. Federhofer, K., "Free Vibrations of Conical Shells," NASA TT F-8261 (1962). Translated from Ingr.-Arch., 9 (1938).

4. Grigolyuk, E. I., "Small Oscillations of Thin Resilient Conical Shells," NASA TT F-25 (1960). Translated from Izves. Akad. Nauk SSSR, O. T. D., No. 6 (1956).

5. Herrmann, G., and Mirsky, I., "On Vibrations of Conical Shells," Journal of Aerospace Science, 25, pp. 451-458 (1958)

6. Shulman, Y., "Vibration and Flutter of Cylindrical and Conical Shells," OSR Tech. Rep. No. 59-776, pp. 22-95 (1959).

7. Saunders, H., Wisniewski, E. J., and Paslay, P. R., "Vibrations of Conical Shells," Journal Acous. Soc. Am., 32, pp. 756-772 (1960).

8. Seide, P., "On the Free Vibrations of Simply Supported Truncated Conical Shells," Conference on Shell Theory and Analysis, Lockheed Missiles and Space Co., Research Lab. (1963).

9. Garnet, H., and Kempner, J., "Axisymmetric Free Vibrations of Conical Shells," ASME Paper No. 64-APM-24, Journal of Applied Mechanics (1964).

10. Goldberg, J. E., Bogdanoff, J. L., and Marcus, L., "On the Calculation of the Axisymmetric Modes and Frequencies of Conical Shells," Journal of Acous. Soc. Am., 32, pp. 738-742 (1960).

11. Goldberg, J. E., Bogdanoff, J. L., and Alspaugh, D. W., "On the Calculation of the Modes and Frequencies of Vibration of Pressurized Conical Shells," AIAA 5th Annual Structural and Materials Conference, Palm Springs, California, pp. 243-249 (1964).

12. Kalnins, A., Free Vibration of Rotationally Symmetric Shells," Journal of Acous. Soc. Am., 36, pp. 1355-1365 (1964).

13. Lindholm, U. S., Kana, D. D., and Abramson, H. N., "Breathing Vibrations of a Circular Cylindrical Shell with an Internal Liquid," Journal of Aerospace Sciences, 29, pp. 1052-1059 (1962).

14. Arnold, R. N. and Warburton, G. B., "The Flexural Vibrations of Thin Cylinders," Journal Proc. Inst. Mech. Eng., 167, pp. 62-74 (1953).